BIOPHYSICS

Electro-mechanical coupling of KCNQ channels is a target of epilepsy-associated mutations and retigabine

Nien-Du Yang[1]†, Richard Kanyo[2]†, Lu Zhao[1], Jingru Li[2], Po Wei Kang[1], Alex Kelly Dou[1], Kelli McFarland White[1], Jingyi Shi[1], Jeanne M. Nerbonne[3], Harley T. Kurata[2]*, Jianmin Cui[1]*

KCNQ2 and KCNQ3 form the M-channels that are important in regulating neuronal excitability. Inherited mutations that alter voltage-dependent gating of M-channels are associated with neonatal epilepsy. In the homolog KCNQ1 channel, two steps of voltage sensor activation lead to two functionally distinct open states, the intermediate-open (IO) and activated-open (AO), which define the gating, physiological, and pharmacological properties of KCNQ1. However, whether the M-channel shares the same mechanism is unclear. Here, we show that KCNQ2 and KCNQ3 feature only a single conductive AO state but with a conserved mechanism for the electro-mechanical (E-M) coupling between voltage sensor activation and pore opening. We identified some epilepsy-linked mutations in KCNQ2 and KCNQ3 that disrupt E-M coupling. The antiepileptic drug retigabine rescued KCNQ3 currents that were abolished by a mutation disrupting E-M coupling, suggesting that modulating the E-M coupling in KCNQ channels presents a potential strategy for antiepileptic therapy.

INTRODUCTION

The KCNQ voltage-gated potassium (Kv) channel family (KCNQ1 to KCNQ5) serves diverse physiological functions, from regulating cardiac action potential duration (*1*, *2*), maintaining epithelial salt homeostasis (*3*), to modulating neuronal excitability (*4*–*6*). Like other Kv channels, KCNQ channels adopt a canonical topology as tetramers, with each α subunit containing six transmembrane segments S1 to S6. S1 to S4 of each α subunit form the voltage-sensing domain (VSD) that senses changes in membrane potential, while S5 and S6 from all four α subunits comprise the central K^+-selective pore (*7*, *8*). Voltage-dependent gating of Kv channels involves three fundamental molecular processes: VSD activation, VSD-pore coupling, and pore opening. In response to membrane depolarization, the positively charged S4 segment moves toward the extracellular space and changes the conformation of the VSD, a process known as "VSD activation." The conformational changes in the VSD then trigger a series of interactions between the VSD and the pore, a process known as "VSD-pore coupling" or "electro-mechanical (E-M) coupling," to open the channel and conduct ionic current.

The VSDs of KCNQ1 activate in two steps upon membrane depolarization: first from the resting state to an experimentally resolvable intermediate state and then proceed to the fully activated state (*9*–*15*). Previous work showed that the KCNQ1 channel opens when its VSDs occupy both the intermediate and fully activated conformations, resulting in two conductive states, the intermediate-open (IO) and activated-open (AO) states (*12*–*18*). The IO and AO states have different properties including channel modulation (*12*), pharmacology (*12*, *14*, *17*, *19*), and regulation by cell signaling (*20*–*22*). Distinctive regulation of the IO and AO states by various KCNE auxiliary subunits causes the channel complex to adopt different balances of IO- and AO-associated properties, underlying tissue-specific KCNQ1 current phenotypes (*12*, *14*).

Our previous studies demonstrated that stepwise VSD activation of KCNQ1 induces pore opening at the IO and AO states via distinctive sets of E-M coupling interactions (*15*). When S4 moves to the intermediate state, the S4-S5 linker interacts with the bottom of the S6 in the same subunit, which is essential for the channel to open to both the IO and AO states. When S4 then transitions to the fully activated state, the S4 and S4-S5 linker of one subunit interact with S5 and S6 of the neighboring subunit. These interactions are important specifically for triggering the pore to open to the AO state. The specific mechanisms of E-M coupling for the two open states provide the basis for some of the IO- and AO-specific properties. For instance, ML277, a KCNQ1 activator, was found to only enhance the AO state occupancy by perturbing the E-M coupling specific for the AO state (*17*). In addition, some disease-associated mutations in KCNQ1 could specifically disable the E-M coupling of individual KCNQ1 open states (*12*, *15*, *16*, *23*).

KCNQ2 and KCNQ3 form the heterotetrameric M-channels (KCNQ2/3) that primarily mediate the M-current in neurons (*4*, *24*). KCNQ4 and KCNQ5 also contribute to M-currents (*5*, *6*). The M-current activates at subthreshold potentials to regulate action potential firing of neurons (*25*, *26*). Reflecting its key role in controlling neuronal excitability, congenital mutations in KCNQ2 and KCNQ3 that alter M-current function are commonly associated with forms of early-onset epilepsy (*27*), including benign familial neonatal convulsions (BFNC) (*28*–*31*) and the more severe early infantile epileptic encephalopathy (EIEE) (*32*–*34*). Activation of M-current hyperpolarizes neurons and suppresses membrane excitability, making the neuronal KCNQ channels prime therapeutic targets against epilepsy. As a result, numerous synthetic compounds specifically targeting neuronal KCNQ channels have been developed (*35*, *36*), such as ztz240 (*37*), ICA069673 (*38*), retigabine (RTG) (*37*, *39*), and ML213 (*40*, *41*). On the other hand, naturally occurring compounds

[1]Department of Biomedical Engineering, Center for the Investigation of Membrane Excitability Disorders, and Cardiac Bioelectricity and Arrhythmia Center, Washington University, St. Louis, MO 63130, USA. [2]Department of Pharmacology, Alberta Diabetes Institute, University of Alberta, Edmonton, AB, Canada. [3]Departments of Developmental Biology and Internal Medicine, Cardiovascular Division, Washington University School of Medicine, St. Louis, MO 63110, USA.
*Corresponding author. Email: jcui@wustl.edu (J.C.); kurata@ualberta.ca (H.T.K.)
†These authors contributed equally to this work.

such as polyunsaturated fatty acids (*42*) and endocannabinoids (*43*) have been recently found as potent KCNQ activators. Among all the compounds, RTG is a first-in-class antiepileptic drug approved for human use as an adjunctive treatment for refractory epilepsy (*44*). A recent study showed that RTG stabilizes both the open conformation of the pore and the activated conformation of the VSD, suggesting an activation mechanism via E-M coupling (*45*). Recent RTG-bound KCNQ structures also revealed that RTG binds at a pocket between adjacent pore segments of the channel and interacts with residues important for E-M coupling (*37*, *39*). These findings make RTG a suitable candidate drug to study the E-M coupling in neuronal KCNQ channels.

KCNQ2 to KCNQ5 share sequence and structure homology as well as many important mechanisms of function with KCNQ1 (*7*, *8*, *37*, *39*, *41*). However, whether the neuronal KCNQ channels also feature two open states in voltage-dependent gating remains elusive, which hinders further understanding of the molecular mechanism for E-M coupling. Furthermore, the link between E-M coupling in neuronal KCNQ channels and human pathophysiology has not been established. Despite extensive studies, whether antiepileptic compounds such as RTG modulates KCNQ channels by altering the E-M coupling has not been fully explored. A deeper understanding of the open state and E-M coupling mechanisms in different KCNQ channels will provide fresh insights into how these channels function and how inherited mutations affecting KCNQ function lead to disease.

In this study, we combined site-directed mutagenesis, electrophysiology, fluorescence measurements, and pharmacology to elucidate the E-M coupling mechanism in neuronal KCNQ2 and KCNQ3 channels. On the basis of the sequence and structure homology between KCNQ1, KCNQ2, and KCNQ3, we designed a set of functional experiments and revealed key similarities and differences in their E-M coupling during voltage-dependent gating. We then took advantage of the antiepileptic prototype drug RTG to demonstrate the impact of modulating E-M coupling in loss-of-function KCNQ2 and KCNQ3 mutants. Our approach and results extend the established framework for KCNQ1 gating mechanism, and build a foundation for understanding the physiological significance, disease pathogenesis, and pharmacological modulation of E-M coupling in neuronal KCNQ channels.

RESULTS

KCNQ2 and KCNQ3 only conduct with fully activated VSD conformation

KCNQ1 to KCNQ3 show high conservation of the VSD including residues critical for voltage-dependent activation (fig. S1A) and are predicted from the sequence alignment to have similar VSD structures. A recent cryo–electron microscopy (cryo-EM) structure of human KCNQ2 (*37*) displays similar S2-S4 registrations within the VSD as the previously published human KCNQ1 cryo-EM structure (*8*), with the charge transfer center residues E2 (E140) (E170 in KCNQ1) and F0 (F137) (F167 in KCNQ1) on S2 and D172 (D202 in KCNQ1) on S3 interacting with gating charge R5 (R210) (H5, H240 in KCNQ1) on S4, indicating conservation of the fully activated VSD conformation (Fig. 1A). The KCNQ3 VSD structure, although not available, is expected to be similar based on sequence homology. Previous structure-function studies have shown that the KCNQ1 VSD sequentially occupies two functionally stable and detectable states during voltage-dependent activation: from the resting to the intermediate and then to the fully activated state (Fig. 1B) (*9*–*15*). KCNQ1 can open when its VSDs adopt either the intermediate or fully activated states, resulting in two open states, the IO and the AO (Fig. 1C) (*12*–*18*). The two open states of KCNQ1 display distinct properties in their activation, pharmacological modulation, and tissue-specific auxiliary subunit regulation (*12*–*18*). However, whether KCNQ2 and KCNQ3 also feature a two-step VSD activation and two open states similar to KCNQ1 is unknown. Throughout our study, we used the expression-optimized $KCNQ3_{A315T}$ mutant (*46*) for homomeric expression of KCNQ3 channels (see Materials and Methods). To track VSD transitions, we used the voltage clamp fluorometry (VCF) technique in KCNQ3, in which the S3-S4 linker of the channel is labeled by a fluorophore, to allow monitoring of VSD movement and pore opening simultaneously during voltage-dependent activation. We developed the KCNQ3 VCF construct $KCNQ3_{A315T/Q218C/L156W/L157F}$ (denoted as KCNQ3*) using aromatic substitutions guided by sequence differences with KCNQ1 that generates larger fluorescence signals compared to previous reports (Fig. 1D and fig. S1, B and C) (*45*) and has minimal effects on channel gating (fig. S1D). We found that KCNQ3* fluorescence-voltage (*F-V*) relation is well fit by a single Boltzmann function and closely overlaps with its conductance-voltage (*G-V*) relation (Fig. 1E). This is consistent with previous KCNQ3 VCF studies (*45*, *47*), although we note that VCF signals from KCNQ3 remain challenging to record, likely underlying slight differences between studies, and challenges with understanding the exact relationship between activation of the VSD and pore opening. In addition, KCNQ3* shows double-exponential current and fluorescence activation kinetics with a small contribution of a slow component (Fig. 1D). A recent VCF study of KCNQ2 showed a similar result (*48*). These results differ from the VCF recordings of KCNQ1, which exhibit two well-separated components in the *F-V* relation (F1 and F2) as the result of the two-step VSD activation (Fig. 1E) (*12*–*18*). Thus, these results suggest that KCNQ2 and KCNQ3 may differ from KCNQ1 by lacking a stable intermediate state of the VSD or two open states. While the intermediate and fully activated VSD conformations have been experimentally determined in KCNQ channels, the resting VSD state remains poorly understood. Despite some functional and modeling studies, the precise conformation of the resting VSD state in KCNQ channels is unclear as it has not been structurally defined. Nevertheless, this did not affect our measurements of VSD movements to the intermediate and fully activated states.

To test whether KCNQ2 and KCNQ3 have only one open state and whether the single open state represents the AO state, we applied a double charge-reversal mutagenesis strategy (*9*, *12*, *14*, *49*, *50*) to arrest KCNQ2 and KCNQ3 VSDs in the fully activated VSD conformation and probed the pore opening of the channels. We generated a series of KCNQ2 and KCNQ3 charge-switching mutants designed to promote electrostatic interactions between specific residue pairs found in the activated VSD structure of KCNQ2 (Fig. 1, A and B) (*37*): F0R (Q2-F137R, Q3-F167R) paired with R5E (Q2-R210E, Q3-R239E) and D172N (Q2-D172N, Q3-D202N) (Fig. 1, G and J). These engineered activated VSD–stabilizing (AO-locked) KCNQ2 and KCNQ3 mutants generated constitutively open channels with minimal voltage dependence (Fig. 1, G and J, and fig. S2, B and D) compared to wild-type KCNQ2 and $KCNQ3_{A315T}$ channels (Fig. 1, F and I, and fig. S2, A and C). This is consistent with the idea that these mutations strongly stabilize the fully activated VSD state for conduction at the constitutive AO state. To also probe whether KCNQ2 and

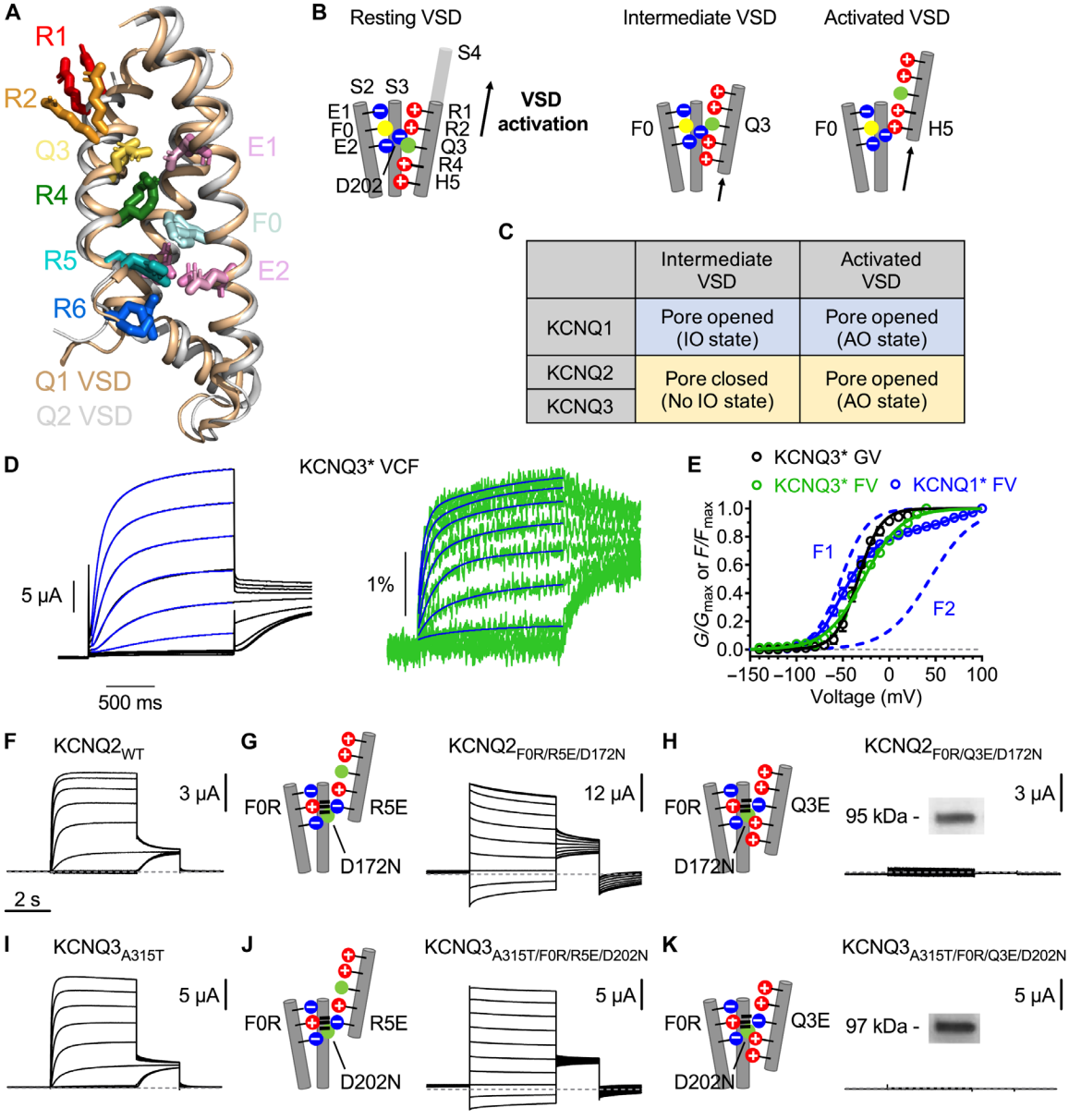

Fig. 1. KCNQ2 and KCNQ3 are only conductive when the VSDs occupy the fully activated conformation. (**A**) Overlay of the human KCNQ1 VSD [Protein Data Bank (PDB): 6UZZ, gold] and KCNQ2 VSD (PDB: 7CR3, silver) cryo-EM structures. R1 to R6: positive gating charges on S4. E1 and E2: negative counter-charges on S2. F0: the aromatic residue on S2. Structures are aligned to S2. S1 is not shown for clarity. (**B**) Cartoons illustrating the key S2-S4 interactions during a two-step KCNQ1 VSD activation. Positive gating charges and polar residues are colored red and green, negative counter charges are colored blue, and F0 on S2 is colored yellow. (**C**) Table summarizing the pore states of KCNQ1-KCNQ3 at the intermediate and fully activated VSD conformations. (**D**) Representative current (black) and fluorescence (green) traces for $KCNQ3_{A315T/Q218C/L156W/L157F}$ (KCNQ3*). Blue lines are double-exponential fits to the activation kinetics. VCF was recorded at holding potential of −140 mV, followed by 1.5-s depolarizing pulses between −140 mV and +60 mV in 10-mV increments, before returning to −20 mV to measure tail currents. (**E**) *G-V* (black) and *F-V* (green) relations of KCNQ3* and *F-V* relation of $KCNQ1_{C214A/G219C/C331A}$ (KCNQ1*) (blue). $V_{1/2}$ and *k* for KCNQ3* *G-V*: −33.5 ± 1.3 mV and 12.2 ± 1.7 mV ($n = 8$), for KCNQ3* *F-V*: −27.6 ± 0.7 mV and 20.3 ± 0.6 mV ($n = 4$), for KCNQ1* F1-V: −51.9 ± 2.7 mV and 14.3 ± 0.4 mV ($n = 5$), and for KCNQ1* F2-V: 43.8 ± 2.7 mV and 23.5 ± 1.7 mV ($n = 5$). (**F** and **I**) Representative current traces for $KCNQ2_{WT}$ and $KCNQ3_{A315T}$. (**G**, **H**, **J**, and **K**) Cartoon schematics and representative current traces of AO- and IO-locked mutants. Insets: Western blot results for membrane expression of the mutants. All traces are shown with 20-mV increments for clarity.

KCNQ3 can conduct at the IO state, we generated another class of charge-switching mutants designed to promote electrostatic interactions between specific residue pairs found in the KCNQ1 intermediate VSD structure (*14*): F0R paired with Q3E (Q2-Q204E, Q3-Q233E) and D172N (Fig. 1, H and K). These intermediate VSD–stabilizing (IO-locked) KCNQ2 and KCNQ3 mutants yielded negligible currents despite robust surface membrane expression as detected by Western blot (Fig. 1, H and K, and fig. S3A), suggesting that the mutant channels could not open. Additional pairs of KCNQ3 IO-locked E2R/R4E (E170R/R236E) and AO-locked E2R/R5E (E170R/R239E) mutants also produced nonfunctional and constitutively open channels, respectively (fig. S2, E and F). Together,

these results suggest that KCNQ2 and KCNQ3 have one steady-state VSD activation from the resting to the fully activated state and conduct only at the AO state. This contrasts with KCNQ1, which features both conductive IO and AO states associated with a two-step VSD activation (Fig. 1C).

Residues important for the AO state E-M coupling are conserved in KCNQ channels

It has been shown that KCNQ1 VSD activation to the intermediate and the fully activated states engages two distinct sets of E-M coupling interactions to induce pore opening, resulting in the IO and AO states (*15*). In particular, our previous studies have identified the E-M coupling interactions specific for the KCNQ1 AO state, which involve residues in the C terminus of S4, the N terminus of the S4-S5 linker, and part of S5 and S6 (*15*). Sequence alignment reveals that most of these residues are conserved in KCNQ2 and KCNQ3 (Fig. 2A), suggesting the conservation of the E-M coupling mechanism specifically for the AO state. In previous studies, we found two disease-associated KCNQ1 mutations W248R and S338F that selectively eliminate the AO state by disabling E-M coupling when the VSDs occupy the fully activated state; however, these mutants remain conductive at the IO state (*15*–*17*). These tryptophan and serine residues are conserved in KCNQ2 and KCNQ3 as well (Fig. 2A), located in the N terminus of the S4-S5 linker and the middle of S6, respectively (Fig. 2B). We therefore made the identical mutations as in KCNQ1 to examine the effects on currents of homomeric KCNQ2 and KCNQ3$_{A315T}$ channels. W218R and S303F mutations in KCNQ2, and W247R and S342F mutations in KCNQ3$_{A315T}$ abolished currents, despite robust expression of the channel proteins in the membrane as detected by Western blot (Fig. 2, C to H, and fig. S3B). In addition, KCNQ2$_{S303F}$ and KCNQ2$_{W218R}$ mutants exerted a dominant-negative effect by strongly suppressing homomeric KCNQ2 currents when coexpressed with wild-type KCNQ2 (fig. S4, A to D). We further carried out VCF experiments and observed robust voltage-dependent fluorescence signals from the KCNQ3*$_{S342F}$ mutant despite diminished current expression (Fig. 2I), demonstrating that the S342F mutation specifically ablates pore opening without eliminating VSD activation. These results together showed that residues specific for the AO state E-M coupling are conserved in KCNQ1 to KCNQ3 channels, and suggest that, in KCNQ2 and KCNQ3, there is no open state other than the AO state when the VSD reaches the fully activated conformation.

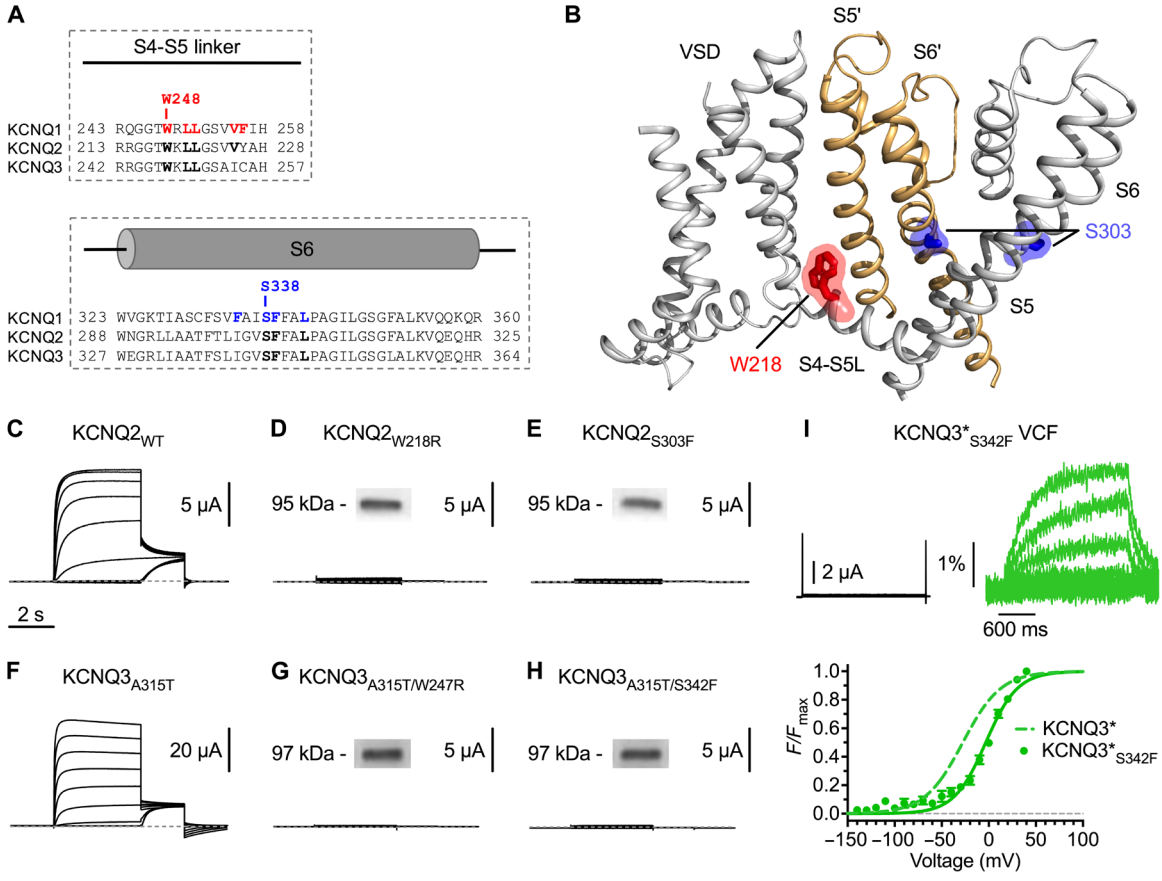

Fig. 2. Residues specific for the AO state E-M coupling are conserved in KCNQ1 to KCNQ3 channels. (**A**) Sequence alignment of KCNQ1 to KCNQ3 S4-S5 linker and S6. Residues important for the KCNQ1 AO state E-M coupling are colored red and blue. Conserved AO state E-M coupling residues in KCNQ2 and KCNQ3 are bolded. (**B**) Conserved AO state E-M coupling residues W218 (red) and S303 (blue) in the human KCNQ2 cryo-EM structure (PDB: 7CR3). S5 and S6 from a neighboring subunit are shown in gold. (**C** to **E**) Representative current traces for KCNQ2$_{WT}$, KCNQ2$_{W218R}$, and KCNQ2$_{S303F}$. (**F** to **H**) Representative current traces for KCNQ3$_{A315T}$, KCNQ3$_{A315T/W247R}$, and KCNQ3$_{A315T/S342F}$. Insets: Western blot results for membrane expression of the mutants. (**I**) Top: Representative current (black) and fluorescence (green) traces for KCNQ3*$_{S342F}$ (KCNQ3* denotes the VCF construct) recorded using the voltage protocol described in Fig. 1D legends. Bottom: *F-V* relation of KCNQ3*$_{S342F}$ (green filled circle). $V_{1/2}$ and *k* for KCNQ3*$_{S342F}$: −3.3 ± 2.1 mV and 16.9 ± 1.7 mV ($n = 6$). Dashed line is the Boltzmann fit for KCNQ3* *F-V* reproduced from Fig. 1E.

KCNQ2 and KCNQ3 exhibit permeant ion regulation and pharmacology homologous to the AO state of KCNQ1

Previous studies in KCNQ1 have shown that IO and AO states have distinct pharmacological sensitivity and modulation by permeating ions (*12*, *14*, *17*). For example, KCNQ1 channels predominantly open to the IO state and exhibit a large Rb^+/K^+ inward tail current ratio of ~3, whereas I_{Ks} channels (KCNQ1 + KCNE1) exclusively open at the AO state and show a much smaller Rb^+/K^+ tail current ratio of ~1, attributed to altered rapid gating transitions in the presence of Rb^+ (*12*, *51*). We compared the ion permeation of KCNQ2 and KCNQ2 + KCNQ3 with the KCNQ1 IO and AO states. By measuring the instantaneous tail current amplitudes of the channels at −60 mV after a +60-mV prepulse for 5 s in 100 mM K^+ or Rb^+ solutions (Fig. 3, A and B), we found that both homomeric KCNQ2 and heteromeric KCNQ2 + KCNQ3 exhibited a small Rb^+/K^+ tail current ratio (Fig. 3E), resembling the KCNQ1 AO state (Fig. 3D) (*12*, *51*). We also tested the ion permeation of a KCNQ2 AO-locked mutant (Fig. 3C) and found that the Rb^+/K^+ tail current ratios were not different from wild-type channels (Fig. 3E). These comparisons suggest that the AO state of KCNQ2 and KCNQ2 + KCNQ3 channels features permeant ion regulation resembling that of the KCNQ1 AO state.

A recent study revealed that the compound C28 differentially affects the IO and AO states in KCNQ1 (*19*). C28 was found to promote KCNQ1 opening by two mechanisms. First, C28 induces a hyperpolarizing shift in the voltage dependence of VSD activation. Second, C28 selectively enhances the E-M coupling of the AO state to increase I_{Ks} currents, but not the IO state so that it does not

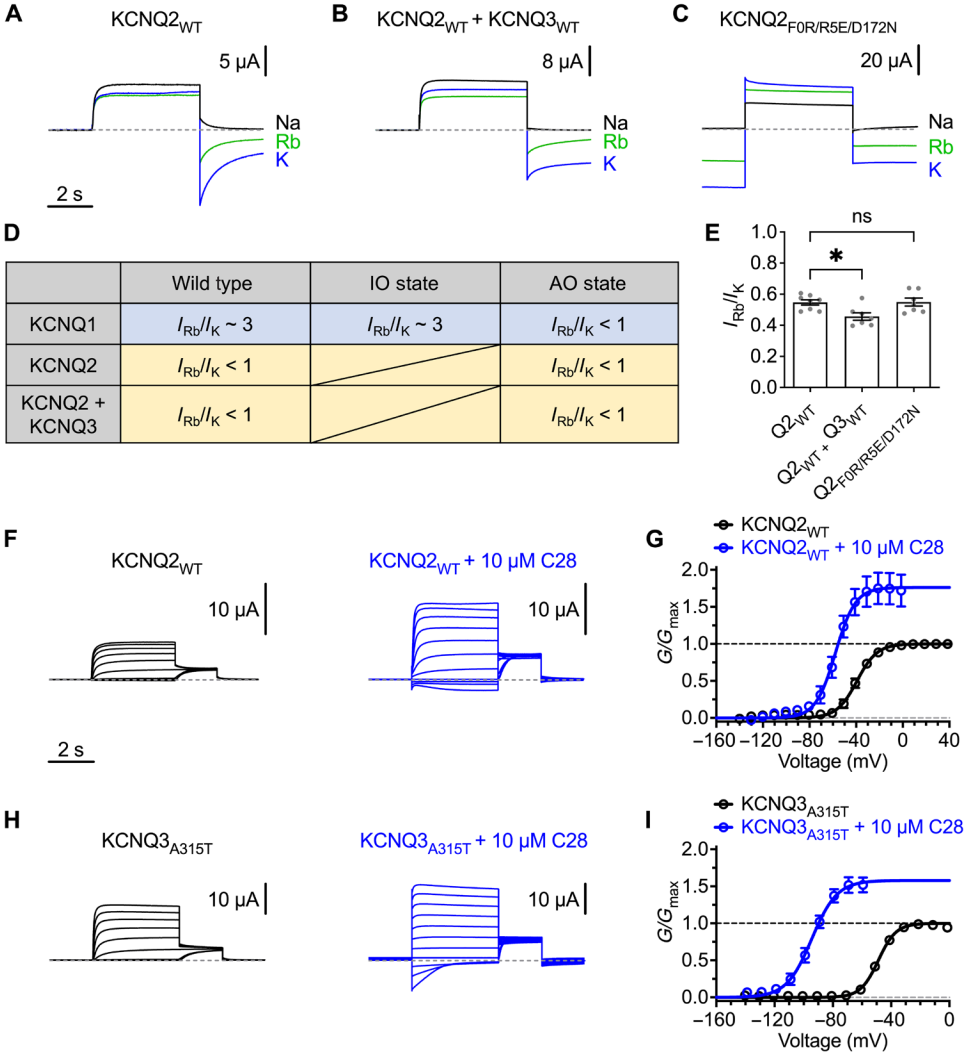

Fig. 3. KCNQ2 and KCNQ3 show permeant ion regulation and pharmacology homologous to the KCNQ1 AO state. Representative current traces for (**A**) $KCNQ2_{WT}$, (**B**) KCNQ2 + KCNQ3, and (**C**) $KCNQ2_{F0R/R5E/D172N}$ recorded in 96 mM Na^+ (black), 100 mM K^+ (blue), or 100 mM Rb^+ (green) external solutions. The tail currents were elicited at −60 mV for 3 s from a prepulse at +60 mV for 5 s. (**D**) Table summarizing the Rb^+/K^+ inward tail current ratios of the open states of KCNQ1, KCNQ2, and KCNQ2/3. (**E**) Average Rb^+/K^+ inward tail current ratios calculated from the instantaneous tail current amplitudes for $KCNQ2_{WT}$ (0.55 ± 0.02, $n = 8$), KCNQ2 + KCNQ3 (0.46 ± 0.02, $n = 7$), and $KCNQ2_{F0R/R5E/D172N}$ (0.55 ± 0.03, $n = 7$). Dots represent individual cells recorded. Statistical significance was determined by one-way analysis of variance (ANOVA) followed by Tukey's post hoc test. ns, not significant. *$P < 0.05$. (**F**) Representative current traces and (**G**) *G-V* relations of $KCNQ2_{WT}$ before and after 10 μM C28. $V_{1/2}$ for control (black): −39.3 ± 2.2 mV ($n = 5$) and for 10 μM C28 (blue): −57.7 ± 2.7 mV ($n = 5$). (**H**) Representative current traces and (**I**) *G-V* relations of $KCNQ3_{A315T}$ before and after 10 μM C28. $V_{1/2}$ for control (black): −48.8 ± 1.1 mV ($n = 5$) and for 10 μM C28 (blue): −94.5 ± 3.2 mV ($n = 5$).

increase KCNQ1 currents (*19*). Since KCNQ2 and KCNQ3 only open to the AO state, we tested if C28 would act similarly to increase the maximum conductance of homomeric KCNQ2 and $KCNQ3_{A315T}$ channels. We found that C28 also activated KCNQ2 and $KCNQ3_{A315T}$ (Fig. 3, F and H) by shifting the *G-V* relation to more negative voltages. At 10 μM C28, the *G-V* shift was ~−18 mV for KCNQ2 as compared to ~−46 mV for $KCNQ3_{A315T}$ (Fig. 3, G and I). Similar to the results in I_{Ks} channels (KCNQ1 AO state) (*19*), C28 increased the maximum conductance of KCNQ2 and $KCNQ3_{A315T}$ by more than 50% (Fig. 3, G and I). Our results together demonstrate that KCNQ2 and KCNQ3 show permeant ion sensitivity and pharmacology that resemble the AO state properties described in KCNQ1.

Disruptions of the AO state E-M coupling in KCNQ2 or KCNQ3 subunits result in loss-of-function phenotypes in the heteromeric M-channel

KCNQ2 and KCNQ3 subunits are important contributors to native "M-current" in neurons (*4*, *24*). When expressed in *Xenopus* oocytes, KCNQ2 coassembles with KCNQ3 to form heteromeric "M-channels" that result in larger currents compared to KCNQ2 homomers alone (Fig. 4, A and B) (*4*). We have previously shown in KCNQ1 channels that the AO state–specific E-M coupling involves interactions between the S4 and S4-S5 linker from one subunit with the S5 and S6 of a neighboring subunit (*15*). In a heteromeric M-channel, the VSD of each KCNQ2 (or KCNQ3) subunit may make substantial contacts with the pore of a neighboring KCNQ3 (or KCNQ2) subunit (*37*). Therefore, the AO state E-M coupling in M-channels is an intersubunit interaction between KCNQ2 and KCNQ3 subunits. With the tools that can selectively disable the AO state E-M coupling in homomeric KCNQ2 or KCNQ3 channels (Fig. 2), we sought to dissect the E-M coupling in heteromeric M-channels. We first examined the impact of KCNQ2 by coexpressing wild-type KCNQ3 with KCNQ2 carrying the AO state–eliminating (AO-less) mutations. Notably, coexpression of the $KCNQ2_{S303F}$ or $KCNQ2_{W218R}$ mutant strongly suppressed M-current amplitude (Fig. 4, C and D). On the other hand, coexpression of wild-type KCNQ2 with the KCNQ3 AO-less mutant $KCNQ3_{S342F}$ or $KCNQ3_{W247R}$ led to weaker suppression of M-current amplitude (Fig. 4, E, F, and I) but shifted the *G-V* relation to more positive voltages compared to wild-type KCNQ2 + KCNQ3 (~+21 and ~+14 mV, respectively) or wild-type KCNQ2 (~+19 and ~+12 mV, respectively) (Fig. 4J). These results suggest that in heteromeric M-channels, the KCNQ2 AO-less mutant subunits strongly abolished channel function, whereas KCNQ3 AO-less mutants modified channel function by reducing current amplitude and shifting the *G-V* relation.

However, the wild-type KCNQ3 and the KCNQ2 AO-less mutants, when expressed alone, all show negligible currents (Fig. 2, D and E) (*46*). Therefore, it was not clear if the KCNQ2 AO-less mutant subunits abolished M-currents (Fig. 4, C and D) by a dominant-negative effect, or instead by failing to associate with wild-type KCNQ3 (which gives rise to little or no current in the absence of KCNQ2 (*46*)). To

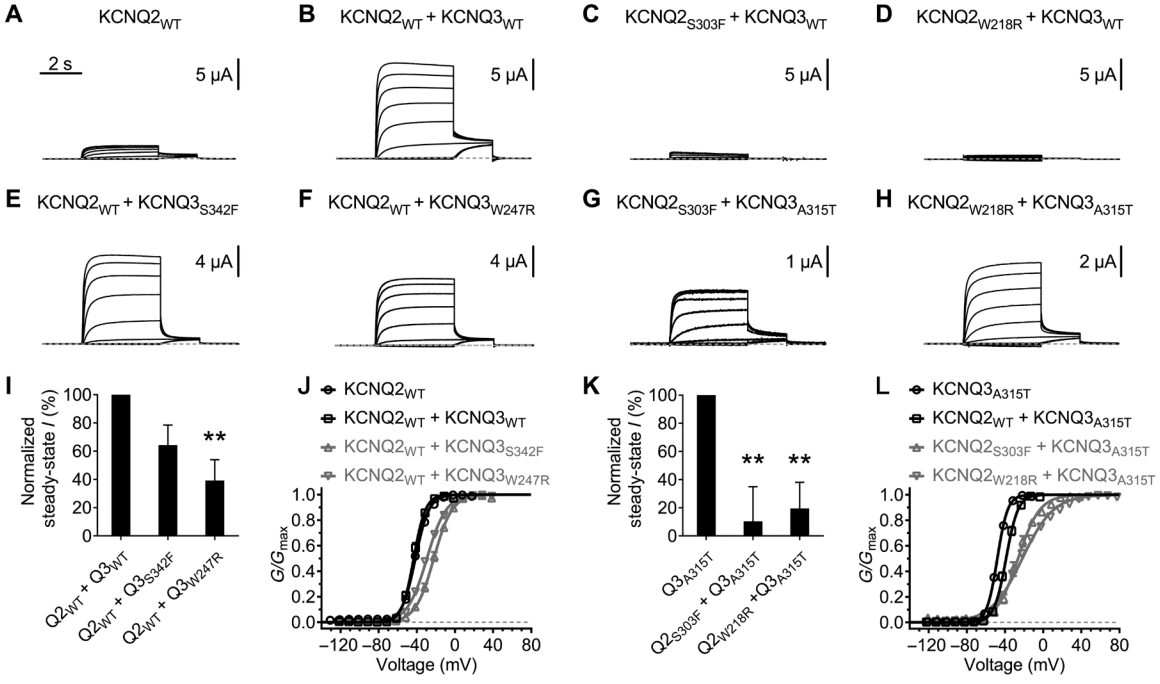

Fig. 4. Mutational disruptions of the AO state E-M coupling in KCNQ2 or KCNQ3 subunits impair the heteromeric M-channel function. Representative current traces for (**A**) $KCNQ2_{WT}$, (**B**) KCNQ2 + KCNQ3, (**C**) $KCNQ2_{S303F}$ + $KCNQ3_{WT}$, (**D**) $KCNQ2_{W218R}$ + $KCNQ3_{WT}$, (**E**) $KCNQ2_{WT}$ + $KCNQ3_{S342F}$, (**F**) $KCNQ2_{WT}$ + $KCNQ3_{W247R}$, (**G**) $KCNQ2_{S303F}$ + $KCNQ3_{A315T}$, and (**H**) $KCNQ2_{W218R}$ + $KCNQ3_{A315T}$. (**I**) Steady-state currents normalized to KCNQ2 + KCNQ3 (100 ± 10.1%, $n = 6$) were 64.3 ± 14.3% ($n = 7$) for $KCNQ2_{WT}$ + $KCNQ3_{S342F}$ and 39.3 ± 14.7% ($n = 7$) for $KCNQ2_{WT}$ + $KCNQ3_{W247R}$. (**J**) *G-V* relations of $KCNQ2_{WT}$ (black open circle), KCNQ2 + KCNQ3 (black open square), $KCNQ2_{WT}$ + $KCNQ3_{S342F}$ (gray open triangle), and $KCNQ2_{WT}$ + $KCNQ3_{W247R}$ (gray open inverted triangle). $V_{1/2}$ for $KCNQ2_{WT}$: −41.5 ± 0.7 mV ($n = 5$), for KCNQ2 + KCNQ3: −43.2 ± 1.0 mV ($n = 6$), for $KCNQ2_{WT}$ + $KCNQ3_{S342F}$: −22.2 ± 1.4 mV ($n = 7$), and for $KCNQ2_{WT}$ + $KCNQ3_{W247R}$: −29.4 ± 0.9 mV ($n = 7$). (**K**) Steady-state currents normalized to $KCNQ3_{A315T}$ (100 ± 11.9%, $n = 5$) were 10.3 ± 24.6% ($n = 5$) for $KCNQ2_{S303F}$ + $KCNQ3_{A315T}$ and 19.5 ± 18.6% ($n = 6$) for $KCNQ2_{W218R}$ + $KCNQ3_{A315T}$. (**L**) *G-V* relations of $KCNQ3_{A315T}$ (black open circle), $KCNQ2_{WT}$ + $KCNQ3_{A315T}$ (black open square), $KCNQ2_{S303F}$ + $KCNQ3_{A315T}$ (gray open triangle), and $KCNQ2_{W218R}$ + $KCNQ3_{A315T}$ (gray open inverted triangle). $V_{1/2}$ for $KCNQ3_{A315T}$: −48.1 ± 0.6 mV ($n = 5$), for $KCNQ2_{WT}$ + $KCNQ3_{A315T}$: −38.9 ± 1.0 mV ($n = 5$), for $KCNQ2_{S303F}$ + $KCNQ3_{A315T}$: −26.3 ± 2.1 mV ($n = 5$), and for $KCNQ2_{W218R}$ + $KCNQ3_{A315T}$: −21.9 ± 1.6 mV ($n = 6$). Statistical significance was determined by Student's *t* test. $^{**}P < 0.01$.

answer this question, we coexpressed KCNQ2 AO-less mutants with $KCNQ3_{A315T}$ to examine their effects on the currents of $KCNQ3_{A315T}$. We found that coexpression of the $KCNQ2_{S303F}$ or $KCNQ2_{W218R}$ mutant suppressed the $KCNQ3_{A315T}$ currents (Fig. 4, G, H, and K) and shifted the *G-V* relation to more positive voltages compared to $KCNQ3_{A315T}$ (~+22 and ~+26 mV, respectively) or wild-type KCNQ2 + $KCNQ3_{A315T}$ (~+13 and ~+17 mV, respectively) (Fig. 4L). The altered voltage dependence (compared to homomeric channels) after mutant subunit coexpression demonstrates that the AO-less mutants of both KCNQ2 and KCNQ3 can coassemble with their counterpart, leading to suppression of heteromeric M-channel function along with altered gating properties. In summary, our findings suggest that disruptions of the AO state E-M coupling by mutations in KCNQ2 or KCNQ3 subunits affect the intersubunit E-M coupling interactions in heteromeric channels to impair M-current function.

Epilepsy-linked mutations in KCNQ2 and KCNQ3 subunits disrupt E-M coupling

Inherited mutations in KCNQ2 and KCNQ3 are frequently associated with neonatal epilepsies (*27*–*34*). To explore whether the AO state E-M coupling in KCNQ2 and KCNQ3 has direct implications for human pathophysiology, we searched the National Center for Biotechnology Information (NCBI) ClinVar database for conserved AO state E-M coupling residues in KCNQ2 and KCNQ3 (Fig. 2A and fig. S5A) identified in patients. Of the ten conserved coupling residues in KCNQ2 (W218, L220, L221, V225, Y237, I238, L241, S303, F304, and L307), we found three mutations [Y237C (*52*), I238V, and F304S (*53*, *54*)] that are associated with EIEE and one mutation (I238L) that is likely pathogenic (fig. S5A). On the other hand, of the nine conserved coupling residues in KCNQ3 (W247, L249, L250, Y266, I267, L270, S342, F343, and L346), we only found one mutation (Y266C) (homologous to Y237C in KCNQ2) (*55*) that is likely pathogenic (fig. S5A). These mutations on S5 and S6 of the channel are in close proximity to each other and to the AO-less mutations (fig. S5B). The $KCNQ2_{F304S}$ mutant, when expressed alone (Fig. 5A) or coexpressed with wild-type KCNQ3 (Fig. 5B), suppressed current amplitude (Fig. 5C) and shifted the *G-V* relation to more positive voltages (shifted ~+31 mV for $KCNQ2_{F304S}$ + $KCNQ3_{WT}$) compared to the wild-type controls (Fig. 5D). On the other hand, the $KCNQ2_{Y237C}$ mutant with or without the coexpression of

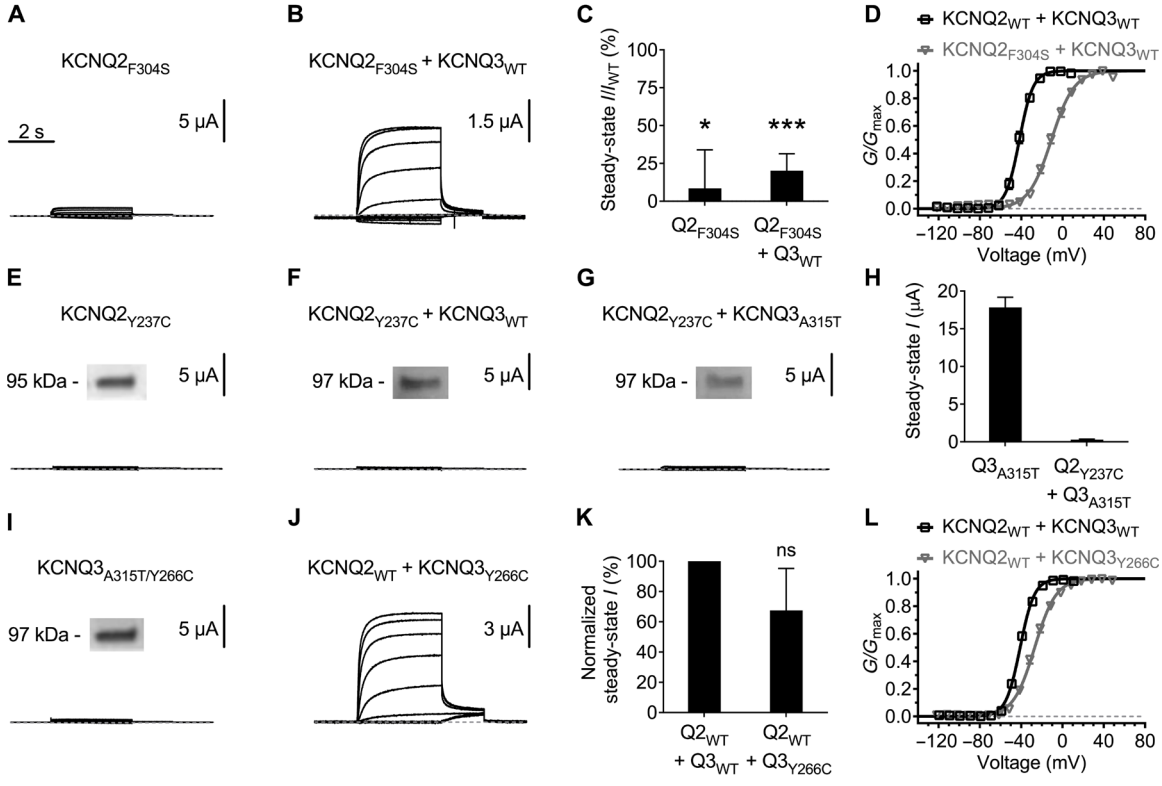

Fig. 5. KCNQ2 and KCNQ3 mutations associated with EIEE disrupt the E-M coupling. (**A** and **B**) Representative current traces for $KCNQ2_{F304S}$ with and without coexpressed $KCNQ3_{WT}$. (**C**) Steady-state currents normalized to $KCNQ2_{WT}$ (100 ± 24.1%, $n = 5$) and KCNQ2 + KCNQ3 (100 ± 4.4%, $n = 6$), respectively, were 8.5 ± 25.4% ($n = 5$) for $KCNQ2_{F304S}$ and 20.2 ± 11.2% ($n = 7$) for $KCNQ2_{F304S}$ + $KCNQ3_{WT}$. (**D**) *G-V* relations of KCNQ2 + KCNQ3 (black open square) and $KCNQ2_{F304S}$ + $KCNQ3_{WT}$ (gray open inverted triangle). $V_{1/2}$ for $KCNQ2_{WT}$ + $KCNQ3_{WT}$: −41.8 ± 1.2 mV ($n = 6$) and for $KCNQ2_{F304S}$ + $KCNQ3_{WT}$: −10.8 ± 1.5 mV ($n = 7$). Currents from $KCNQ2_{F304S}$ alone were too small to obtain reliable *G-V* relations. (**E** to **G**) Representative current traces for $KCNQ2_{Y237C}$ alone, or coexpressed with $KCNQ3_{WT}$, or $KCNQ3_{A315T}$. Insets: Western blots for membrane expression of the mutants. For $KCNQ2_{Y237C}$ + $KCNQ3_{WT}$ and $KCNQ2_{Y237C}$ + $KCNQ3_{A315T}$, the KCNQ3 protein was probed. (**H**) Steady-state current amplitudes were 17.8 ± 1.4 μA ($n = 4$) for $KCNQ3_{A315T}$ and 0.3 ± 0.1 μA ($n = 10$) for $KCNQ2_{Y237C}$ + $KCNQ3_{A315T}$. (**I** and **J**) Representative current traces for $KCNQ3_{Y266C}$ alone or coexpressed with $KCNQ2_{WT}$. Inset: Western blot results for membrane expression of the mutant. (**K**) Steady-state currents normalized to KCNQ2 + KCNQ3 (100 ± 21.2%, $n = 6$) were 67.6 ± 27.8% ($n = 5$) for $KCNQ2_{WT}$ + $KCNQ3_{Y266C}$. (**L**) *G-V* relations of KCNQ2 + KCNQ3 (black open square) and $KCNQ2_{WT}$ + $KCNQ3_{Y266C}$ mutant (gray open inverted triangle). $V_{1/2}$ for $KCNQ2_{WT}$ + $KCNQ3_{WT}$: −41.0 ± 0.9 mV ($n = 6$) and for $KCNQ2_{WT}$ + $KCNQ3_{Y266C}$: −26.9 ± 1.3 mV ($n = 5$). Statistical significance was determined by Student's *t* test. *$P < 0.05$; ***$P < 0.001$.

wild-type KCNQ3 resulted in near-complete suppression of currents despite robust expression of the channel protein detected in the membrane (Fig. 5, E and F, and fig. S3C). Coexpression of the mutant with $KCNQ3_{A315T}$ also strongly suppressed the currents of $KCNQ3_{A315T}$ channels (Fig. 5, G and H, and fig. S3C), producing a more severe loss-of-function phenotype than our designed AO-less mutants (Fig. 4, G, H, and K). With the homologous mutation on $KCNQ3_{A315T}$, $KCNQ3_{A315T/Y266C}$ alone abolished the currents without preventing the expression of the channel protein to the membrane (Fig. 5I and fig. S3C), suggesting that it functions as an AO-less mutant (similar to Fig. 2, G and H). Coexpression of the $KCNQ3_{Y266C}$ mutant with wild-type KCNQ2 did not significantly affect the M-current amplitude (Fig. 5, J and K) but shifted the *G-V* relation to more positive voltages (shifted ~+14 mV) compared to the wild-type KCNQ2 + KCNQ3 (Fig. 5L), mirroring the effects of our designed AO-less mutants (Fig. 4, E, F, I, and J). Mutants $KCNQ2_{I238V}$ and $KCNQ2_{I238L}$, however, were found to have mild effects on the current amplitude (fig. S5, C to E and G to I) and the *G-V* relation when expressed alone (shifted ~+12 and ~+5 mV, respectively) or coexpressed with wild-type KCNQ3 (shifted ~+4 and ~+7 mV, respectively) (fig. S5, F and J). To mimic heterozygosity of disease-linked mutations, we coexpressed the KCNQ2 mutants with wild-type KCNQ2 and KCNQ3 subunits in a 0.5:0.5:1 ratio. In this configuration, $KCNQ2_{F304S}$ moderately suppressed M-current amplitude (fig. S4, E, F, and I) and shifted the *G-V* relation (~+12 mV) compared to the wild-type control (fig. S4J), whereas $KCNQ2_{Y237C}$ exerted a dominant-negative effect that strongly suppressed M-current amplitude (fig. S4, E, G, and I). Coexpression of $KCNQ3_{Y266C}$ mutant with wild-type KCNQ3 and KCNQ2 in a 0.5:0.5:1 ratio produced a small shift (~+6 mV) in *G-V* relation (fig. S4J) and did not significantly affect the M-current amplitude (fig. S4, E, H, and I). These results together demonstrate the physiological importance of the AO state and suggest that disrupting the AO state E-M coupling in KCNQ2 and KCNQ3 is a mechanism contributing to some neonatal epilepsies.

Retigabine rescues the currents of KCNQ3 mutant by restoring the E-M coupling

RTG is the first voltage-gated K^+ channel activator approved for clinical use as an antiepileptic drug (*44*), and it specifically activates KCNQ2 to KCNQ5 channels by shifting the voltage dependence of channel opening to more negative potentials (*56*, *57*). Previous studies have suggested that RTG binds to the pore domain of the channels through interactions with several residues and demonstrated that a conserved tryptophan residue in the S5 helix (W236 in KCNQ2; W265 in KCNQ3) is essential for RTG effects (*40*, *58*–*60*). Consistent with functional studies, a recent cryo-EM structure of human KCNQ2 in complex with RTG (*37*) revealed that RTG binds at the intersubunit interface of the channel pore domain, by mainly forming hydrogen bonds with the side chain of W236, S303, and the main-chain carbonyls of L299 and F305, as well as hydrophobic interactions with residues W236, F240, L243, L272, L299, F304, and F305. We found that several RTG-interacting residues overlap (or are in close proximity) with residues important for the AO state E-M coupling (such as S303 and F304) (Fig. 6A and fig. S5A), suggesting that RTG may directly modulate E-M coupling in KCNQ2 and KCNQ3. We therefore examined the effects of RTG on the E-M coupling in KCNQ3 using the AO-less mutant $KCNQ3_{A315T/S342F}$ (equivalent to $KCNQ2_{S303F}$). Application of a saturating concentration (100 μM) of RTG led to a partial rescue of $KCNQ3_{A315T/S342F}$ currents (Fig. 6B). For $KCNQ3_{A315T}$ channels, 100 μM RTG produced a large hyperpolarizing shift (~−52 mV) in the *G-V* relation; however, the voltage dependence of activation of the RTG-rescued $KCNQ3_{A315T/S342F}$ channels was notably right-shifted compared to $KCNQ3_{A315T}$ (Fig. 6C), suggesting that RTG partially restored channel function in the mutant. We also carried out VCF experiments in the presence and absence of RTG using a voltage protocol that highlights kinetics of VSD deactivation, which are prominently affected by RTG (Fig. 6D). Consistent with a previous report (*45*), KCNQ3* *G-V* and *F-V* relations closely overlapped and exhibited similar RTG-mediated shifts to negative potentials (~−47 mV), suggesting that RTG binding within the pore domain can be readily transduced to the VSD via the tight coupling between pore opening and VSD activation (Fig. 6E). The AO-less $KCNQ3*_{S342F}$ mutant exhibited no currents under control condition but retained robust fluorescence signals (Figs. 2I and 6D). In the presence of 100 μM RTG, the *F-V* relation of $KCNQ3*_{S342F}$ was slightly shifted by ~−15 mV (Fig. 6E), consistent with partial restoration of the coupling between pore opening and VSD activation. The difference in the coupling between pore opening and VSD activation was also revealed by VSD kinetics. Similar to previous studies (*45*), RTG affected the KCNQ3* VSD kinetics by slowing the VSD deactivation rate (Fig. 6, D and F), which is consistent with RTG binding to the pore domain and altering the E-M coupling. Compared to KCNQ3*, $KCNQ3*_{S342F}$ showed a much faster VSD deactivation kinetics (Fig. 6, D and F). This effect is comparable to previously reported proximal C terminus mutations in KCNQ3 that uncoupled the pore and the VSD (*45*) and may reflect the differences in VSD function when the influence of the pore was weakened by the S342F mutation. RTG also slowed the VSD deactivation rate of $KCNQ3*_{S342F}$ but to a much lesser extent compared to KCNQ3* (Fig. 6, D and F), suggesting that RTG may restore some of the E-M coupling. Together, these results suggest that RTG interacts with critical residues to directly modulate the E-M coupling in KCNQ2 and KCNQ3. When the E-M coupling is intact ($KCNQ3_{A315T}$), transduction of RTG binding from the pore to the VSD is robust and efficient. On the other hand, when the E-M coupling is abolished ($KCNQ3_{A315T/S342F}$), RTG can restore the E-M coupling to partially rescue channel function, but fails to have the same influence on the voltage dependence of VSD activation and VSD deactivation kinetics.

Retigabine rescues some epilepsy-associated KCNQ2 and KCNQ3 mutants by modulating the E-M coupling

We then further explored if RTG can rescue disease-linked KCNQ2 and KCNQ3 mutants with compromised E-M coupling (Fig. 5). These epilepsy-associated mutations are located near or within the binding pocket of RTG (Fig. 6A), suggesting that RTG may modulate the E-M coupling of these mutants. For the $KCNQ3_{A315T/Y266C}$ mutant (*55*) that behaves similarly to our designed KCNQ3 AO-less mutants (Fig. 2, G and H) and abolished the currents when expressed alone (Figs. 5I and 7A), 100 μM RTG was able to rescue a small but significant K^+ current relative to control condition (Fig. 7, A and B), reflecting a partial restoration of the E-M coupling by RTG. When the $KCNQ3_{Y266C}$ mutant is coexpressed with wild-type KCNQ2, 100 μM RTG shifted the voltage dependence of channel opening (by ~−17 mV) to a level similar to wild-type KCNQ2 + KCNQ3 channels and increased the maximum conductance (by >40%) (Fig. 7, C and D). We found that 100 μM RTG also enhanced the currents of the EIEE-linked $KCNQ2_{F304S}$ mutant

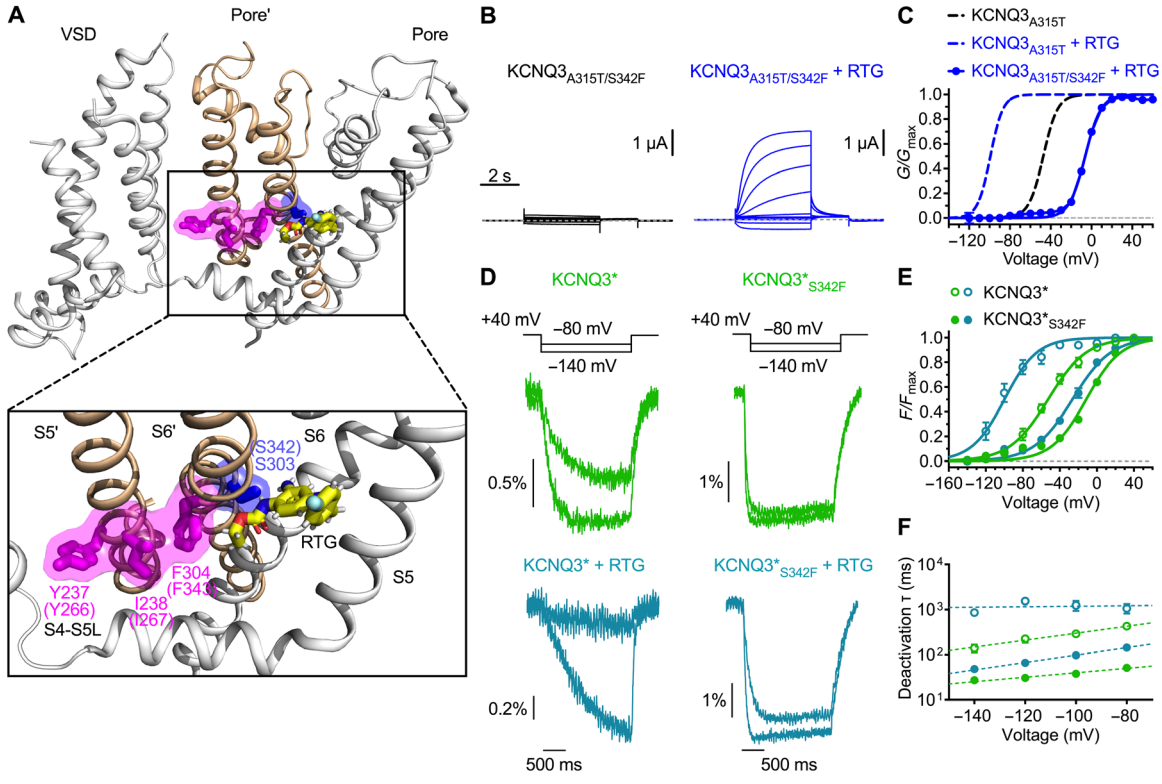

Fig. 6. Retigabine restores E-M coupling to rescue the currents of AO-less KCNQ3 mutant. (**A**) Mapping the key AO state E-M coupling residue S303 (blue) and the EIEE-associated residues Y237, I238, and F304 (magenta) onto the retigabine-bound human KCNQ2 cryo-EM structure (PDB: 7CR7). Brackets indicate amino acid numbers for KCNQ3. S5 and S6 from a neighboring subunit are shown in gold. (**B**) Representative current traces and (**C**) *G-V* relations of $KCNQ3_{A315T/S342F}$ before and after 100 μM retigabine. $V_{1/2}$ for $KCNQ3_{A315T/S342F}$ with 100 μM retigabine (blue filled circle): −6.2 ± 1.0 mV (n = 9). Dashed lines are fits for $KCNQ3_{A315T}$ with $V_{1/2}$ for control (black): −47.3 ± 0.8 mV (n = 5) and 100 μM retigabine (blue): −99.2 ± 1.9 mV (n = 5). (**D**) Representative fluorescence deactivation traces of KCNQ3* and $KCNQ3^*_{S342F}$ before (green) and after (cyan) 100 μM retigabine. (**E**) *F-V* relations of KCNQ3* and $KCNQ3^*_{S342F}$ before and after 100 μM retigabine. $V_{1/2}$ for KCNQ3* control (green open circle): −52.7 ± 4.6 mV (n = 4), for KCNQ3* with 100 μM retigabine (cyan open circle): −99.8 ± 5.9 mV (n = 3), for $KCNQ3^*_{S342F}$ control (green filled circle): −11.5 ± 0.2 mV (n = 6), and for $KCNQ3^*_{S342F}$ with 100 μM retigabine (cyan filled circle): −26.4 ± 1.4 mV (n = 8). (**F**) Fluorescence deactivation time constants of KCNQ3* and $KCNQ3^*_{S342F}$ before and after 100 μM retigabine. Dotted lines are semi-log line fits. VCF was recorded using the deactivation voltage protocol illustrated at the top of (D).

(*53*, *54*) + wild-type KCNQ3 channels (Fig. 7E) by shifting the *G-V* relation to more negative potentials (~−43 mV) and increasing the maximum conductance (by >25%) (Fig. 7F). To estimate the outcome in heterozygous conditions, we performed RTG experiments in channel configurations that mimic the genetic balance of the disease-linked mutants. When $KCNQ2_{F304S}$ is coexpressed with wild-type KCNQ2 and KCNQ3 subunits in a 0.5:0.5:1 ratio, RTG enhanced the currents by shifting the *G-V* relation to more negative potentials (~−43 mV) (fig. S6A) and increasing the maximum conductance (~2-fold) (fig. S6B). Similarly, when $KCNQ3_{Y266C}$ is coexpressed with wild-type KCNQ3 and KCNQ2 subunits in a 0.5:0.5:1 ratio, RTG potentiated the currents by shifting the voltage dependence of opening (by ~−41 mV) (fig. S6A) and increasing the maximum conductance (~2.5-fold) (fig. S6B). Despite the profound effects of RTG on some of the disease-linked mutants and $KCNQ3_{A315T/S342F}$ (Fig. 6), RTG did not rescue the currents of $KCNQ2_{W218R}$, $KCNQ2_{Y237C}$, $KCNQ2_{S303F}$, or $KCNQ3_{A315T/W247R}$ mutant (fig. S6C). Together, these results demonstrate that RTG can rescue KCNQ2 and KCNQ3 mutants with disrupted E-M coupling and suggest that other small-molecule KCNQ openers with similar mechanisms to modulate E-M coupling can benefit the treatment of some neonatal epilepsies.

DISCUSSION

Elucidating the molecular mechanism for E-M coupling is an important step toward understanding the voltage-dependent gating of Kv channels. Recent structure-function studies revealed that the KCNQ1 channel features a two-stage hand-and-elbow E-M coupling mechanism (*15*), where two steps of VSD activation, from the resting to intermediate and lastly to the fully activated state (*9*–*15*), trigger two sets of E-M coupling interactions that generate two distinct conductive IO and AO states (fig. S7A) (*12*–*18*). This E-M coupling mechanism and the regulation of the IO and AO states define the gating, pharmacology, physiology, and pathophysiology of KCNQ1 (fig. S7) (*12*–*18*). KCNQ2 to KCNQ5 are homologous to KCNQ1 in structure (*7*, *8*, *37*, *39*, *41*) and share important characteristics of gating mechanism with KCNQ1, such as dependence on phosphatidylinositol 4,5-bisphosphate (PIP_2) (*23*, *61*, *62*) and calmodulin (*63*–*65*). However, whether the KCNQ2-KCNQ5 channels share the same E-M coupling mechanism in their voltage-dependent gating with KCNQ1 remains unclear. In this study, we provided functional evidence that the neuronal homolog KCNQ2 and KCNQ3 channels are different from KCNQ1 in which they feature a single AO state but with a conserved E-M coupling mechanism specific for the AO state (Figs. 1 to 3 and fig. S7A). We showed that the AO

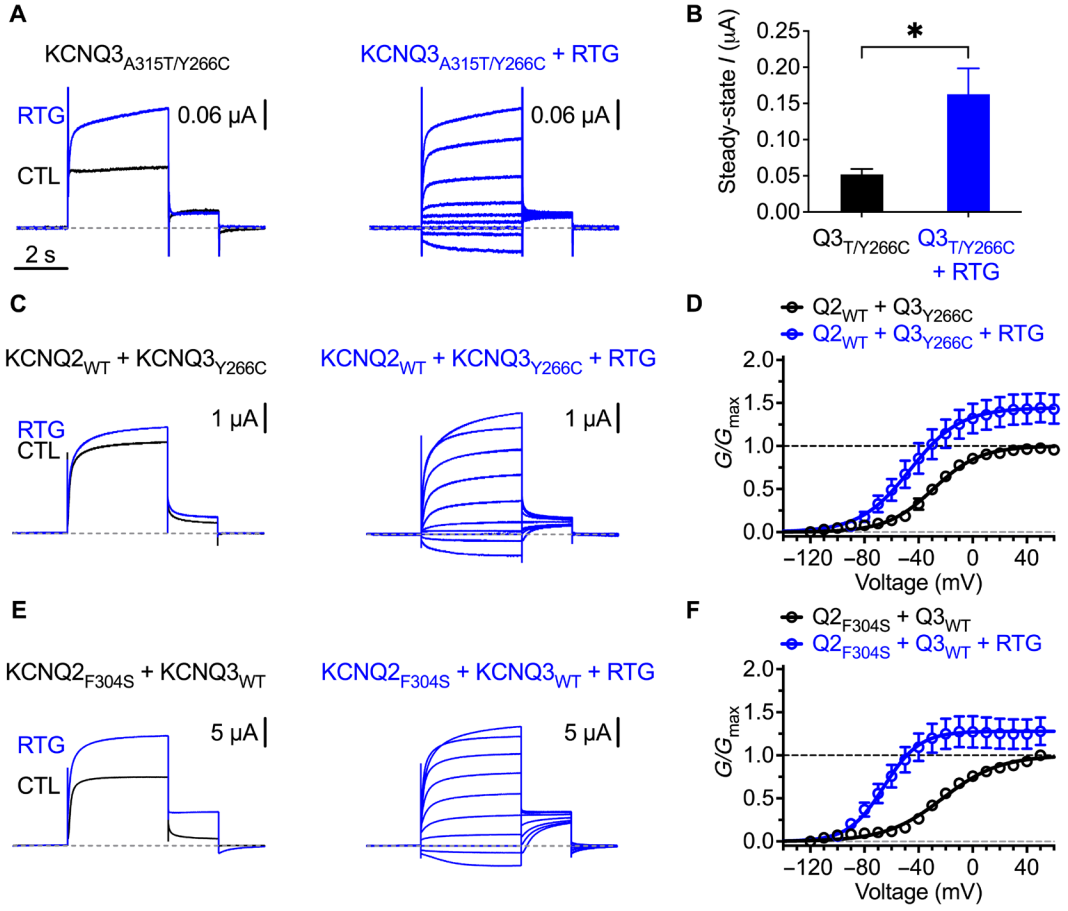

Fig. 7. Retigabine modulates the E-M coupling to rescue epilepsy-linked mutants of KCNQ2 and KCNQ3. (**A**) Representative current traces of $KCNQ3_{A315T/Y266C}$ before (black) and after (blue) 100 μM retigabine. Single traces at +40 mV (left) and all traces after retigabine (right) are shown. (**B**) Steady-state current amplitudes of $KCNQ3_{A315T/Y266C}$ were 0.05 ± 0.01 μA ($n = 4$) for control (black) and 0.16 ± 0.04 μA ($n = 4$) for 100 μM retigabine (blue). Statistical significance was determined by paired Student's *t* test. *$P < 0.05$. (**C**) Representative current traces of $KCNQ2_{WT} + KCNQ3_{Y266C}$ before (black) and after (blue) 100 μM retigabine. Single traces at +40 mV (left) and all traces after retigabine (right) are shown. (**D**) *G-V* relations of $KCNQ2_{WT} + KCNQ3_{Y266C}$ before and after 100 μM retigabine. $V_{1/2}$ for control (black): −29.2 ± 2.9 mV ($n = 4$) and for 100 μM retigabine (blue): −46.4 ± 9.4 mV ($n = 4$). (**E**) Representative current traces of $KCNQ2_{F304S} + KCNQ3_{WT}$ before (black) and after (blue) 100 μM retigabine. Single traces at +40 mV (left) and all traces after retigabine (right) are shown. (**F**) *G-V* relations of $KCNQ2_{F304S} + KCNQ3_{WT}$ before and after 100 μM retigabine. $V_{1/2}$ for control (black): −22.2 ± 2.6 mV ($n = 5$) and for 100 μM retigabine (blue): −65.5 ± 6.0 mV ($n = 5$).

state E-M coupling of M-channels is physiologically important and is a target of epilepsy-associated mutations (Figs. 4 and 5 and fig. S7A). Last, we took advantage of a well-studied neuronal KCNQ channel opener RTG to demonstrate that modulating the AO state E-M coupling holds therapeutic potential against congenital epilepsy (Figs. 6 and 7). This work is built on the foundation of a well-established mechanistic framework for KCNQ1 gating (*12*–*18*) and strengthens our understanding of the role of E-M coupling in physiology, pathophysiology, and pharmacology of KCNQ channels.

Recent cryo-EM structures revealed that the neuronal KCNQ channels share similar VSD conformations with KCNQ1, representing the conserved fully activated VSD state (Fig. 1A) (*7*, *8*, *37*, *41*). Consistent with other studies (*45*, *47*, *48*), our VCF results showed that KCNQ3, unlike KCNQ1, exhibits a one-step VSD transition based on steady-state voltage-dependent activation (Fig. 1, D and E). We then demonstrated with VSD-arresting charge-switching mutations that KCNQ2 and KCNQ3 only conduct in the AO state when the VSDs occupy the fully activated conformation (Fig. 1, F to K), contrasting the two open states of KCNQ1 (*12*–*18*). Mutations that target the AO state E-M coupling completely abolished the currents (Fig. 2), further supporting the idea that KCNQ2 and KCNQ3 only feature an AO state. This conserved single AO state defines the properties of KCNQ2 and KCNQ3 channels, including the mechanism of E-M coupling, sensitivity to permeant ions, and pharmacology (Figs. 2 and 3), which are similar to the AO state of the KCNQ1 channel (fig. S7) (*12*, *15*–*17*, *19*).

Although KCNQ2 and KCNQ3 predominantly activate with a fully activated VSD conformation, some differences with AO state properties of KCNQ1 should be noted. First, the AO-only KCNQ2 and KCNQ3 channels have a negative $V_{1/2}$ (~−40 mV) of *G-V* relations and fast activation kinetics that resemble KCNQ1, which is IO-predominant. In contrast, the KCNQ1 AO state exhibits a right-shifted *G-V* relation ($V_{1/2}$ ~ +40 mV) and slower activation kinetics (*12*–*18*, *64*) compared to KCNQ2 and KCNQ3 (Fig. 1, D and E) (*45*, *47*, *48*). While these differences in the AO state activation properties may have important implications for the primary physiological roles of KCNQ2/3 (regulation of neuronal excitability) (*25*, *26*) versus KCNQ1 (cardiac action potential repolarization) (*1*, *2*), it remains

unclear why the gating features of KCNQ2 and KCNQ3 resemble the KCNQ1 IO state, instead of the AO state. It will be interesting for future studies to elucidate whether and how the differences in AO voltage dependence and kinetics between KCNQ2/3 and KCNQ1 derive from the VSDs of these channels.

While the steady-state *F-V* relation only indicated one-step VSD movement for KCNQ2 and KCNQ3 (Fig. 1E) (*45*, *47*, *48*), it should be noted that the possibility of a transient "intermediate state" existing during VSD activation cannot be totally ruled out. It is possible that such a VSD state may be kinetically observable based on biexponential kinetics of VSD activation (Fig. 1D and fig. S7A), but not stable enough to be detected in the steady state *F-V* (Fig. 1E), nor sufficient to generate channel opening (fig. S7A). Two-step VSD activation is a common feature in Kv channels. Besides KCNQ1, a similar example is the *Drosophila* Shaker channel that exhibited two steps in the kinetics and steady state of VSD activation (*66*, *67*). Some mutations in the Shaker channel were found to separate the two VSD activation steps even more (*68*–*70*). However, unlike KCNQ1, the Shaker channel only has one open state and no pore opening at the intermediate VSD state (*71*). Here, we showed that KCNQ2 and KCNQ3 are homologous to KCNQ1 but only feature one open state as well (Figs. 1 to 3). These comparisons suggest that one open state at the fully activated VSD conformation is the canonical mechanism in Kv channels, whereas the two open states in KCNQ1 are an exception. The reason for the two KCNQ1 open states is not clear and remains an important subject for future studies. The E-M coupling interactions specific for the AO state are conserved in KCNQ2 and KCNQ3, suggesting that the mechanism likely applies to many other domain-swapped Kv channels.

Besides the protein-protein interactions investigated in this study, PIP_2-mediated interactions are also important for E-M coupling. In KCNQ channels, depletion of PIP_2 closes channels (*23*, *45*, *62*). We have previously shown in KCNQ1 that this is due to the disruption of PIP_2-mediated VSD-pore coupling (*23*). On the other hand, in the presence of PIP_2, mutations that target the protein-protein E-M coupling also render nonfunctional channels (*15*). These results suggest that both classes of interactions are important for E-M coupling. Previous functional studies in KCNQ1 and KCNQ3 (*23*, *45*, *61*) as well as recent PIP_2-bound KCNQ1 and KCNQ4 structures (*8*, *41*) have revealed a conserved PIP_2 binding pocket responsible for PIP_2-mediated VSD-pore coupling in KCNQ channels (fig. S8A). Mapping the PIP_2 binding sites and the sites important for protein-protein E-M coupling onto the human KCNQ2 structure revealed that they are spatially distinct (fig. S8B). However, the close proximity between the two sites (fig. S8B) suggests that the two E-M coupling mechanisms may interact allosterically to affect each other. Therefore, the possibility of allosteric effects of AO-disrupted mutations on PIP_2 binding cannot be totally ruled out (*72*). In addition, since RTG also regulates E-M coupling, it is conceivable that PIP_2 may modulate RTG effects (*45*, *73*).

The AO-only feature and its specific E-M coupling mechanism define not only the properties of homomeric KCNQ2 and KCNQ3 channels but also KCNQ2 in complex with KCNQ3, which is the major form of the M-channels in neurons (*4*). The sensitivity to permeant ions and pharmacology of the M-channels are similar to those of KCNQ2 and KCNQ3 (Fig. 3) (*19*, *74*). The E-M coupling specific for the AO state is also physiologically important, as demonstrated by the coexpression of KCNQ2 or KCNQ3 subunits carrying the AO-less mutations with their wild-type counterparts (Fig. 4). Disrupting the E-M coupling in KCNQ2 versus KCNQ3 has differential consequences to the M-channel function (Fig. 4). This result may have some implications for why we observe far more disease-associated mutations in KCNQ2 compared to KCNQ3 and for the severity of disease manifestations. For instance, most BFNC mutations are found in KCNQ2 with less mutations identified in KCNQ3, whereas the EIEE mutations that cause a more severe form of childhood epilepsy are far more predominant in KCNQ2 (*31*, *75*). It should be noted that differential expression of KCNQ2 and KCNQ3 during development (expression of KCNQ2 preceding that of KCNQ3) (*76*) may also underlie the higher pathogenic impact of KCNQ2 versus KCNQ3 variants. The AO state and its E-M coupling mechanism not only defines the fundamental properties of the M-channel (Figs. 3 and 4) but also is a target in disease pathology as several epilepsy-associated mutations were found to disrupt the E-M coupling (Fig. 5 and figs. S4 and S7A). Last, we demonstrated with a small-molecule drug RTG that the E-M coupling could be specifically modulated to rescue the currents of a KCNQ3 AO-less mutant (Fig. 6 and fig. S7B) and the function of diseased M-channels (Fig. 7 and fig. S6), suggesting that targeting the conserved AO state E-M coupling is a potential antiepileptic strategy.

MATERIALS AND METHODS

Constructs and mutagenesis

Site-directed mutations were introduced into KCNQ2 and KCNQ3 channels using overlap extension and high-fidelity polymerase chain reaction (PCR). The presence of all desired mutations was verified by DNA sequencing. The complementary RNA (cRNA) of the channels was synthesized by in vitro transcription using the mMessage mMachine T7 or SP6 polymerase kit (Applied Biosystems–Thermo Fisher Scientific). In experiments involving homomeric expression of KCNQ3 channels, the A315T mutation was introduced to enable efficient trafficking and functional expression of KCNQ3 channels (*46*).

Xenopus oocyte channel expression

Stage V-VI oocytes were obtained from *Xenopus laevis* by laparotomy procedure in accordance with the protocols approved by the Washington University Animal Studies Committee (protocol #20190030) and by the University of Alberta Animal Care Committee (protocol #AUP00001752). Oocytes were digested with collagenase (0.5 mg/ml; Sigma-Aldrich, St. Louis, MO) to remove the follicle cell layer. A total of 9.2 ng of channel cRNA was then injected into each oocyte using Nanoject (Drummond, Broomall, PA). For experiments involving coexpression of KCNQ2 and KCNQ3, cRNAs were coinjected at 1:1 (KCNQ2:KCNQ3) mass ratio, unless otherwise specified. For VCF experiments, all injected cRNA amounts were doubled to attain higher surface expression level. The injected oocytes were incubated at 18°C for at least 2 days in ND96 solution [96 mM NaCl, 2 mM KCl, 1.8 mM $CaCl_2$, 1 mM $MgCl_2$, 5 mM Hepes, 2.5 mM Na pyruvate, and 1% penicillin-streptomycin (pH 7.6)] before recording.

Two-electrode voltage clamp and VCF

Microelectrodes were pulled from thin wall borosilicate glass (item #B150-117-10, Sutter Instrument, Novato, CA) by a micropipette puller (P-97 or P-1000, Sutter Instrument, Novato, CA) to a resistance of 0.5 to 3 megohms when filled with 3 M KCl solution. Whole-cell ionic currents were recorded from oocytes bathed in ND96 solution

using a CA-1B amplifier (Dagan, Minneapolis, MN) in two-electrode voltage clamp (TEVC) mode. Signals were sampled at 1 kHz and low-pass–filtered at 2 kHz using the Patchmaster software (HEKA, Holliston, MA). Unless otherwise specified, currents were recorded at holding potential of −80 mV, followed by 4-s depolarizing pulses stepping from −120 to +60 mV in 10-mV increments, before returning to −40 mV for 2 s to measure tail currents. For ion permeation experiments, 100 mM K^+ [100 mM KCl, 1.8 mM $CaCl_2$, 1 mM $MgCl_2$, and 5 mM Hepes (pH 7.6)] or 100 mM Rb^+ [96 mM RbCl, 4 mM KCl, 1.8 mM $CaCl_2$, 1 mM $MgCl_2$, and 5 mM Hepes (pH 7.6)] solutions were perfused onto oocytes to steady state. For experiments comparing the current amplitudes, cRNAs encoding wild-type and mutant channels were injected on the same day. The injected oocytes were later recorded on the same day to control for channel expression and allow for current amplitude comparison between wild-type and mutant channels. For VCF (*45*), oocytes expressing channels were labeled for 20 min on ice with 200 μM Alexa Fluor 488 C5-maleimide (Thermo Fisher Scientific, Waltham, MA) in high K^+ depolarizing solution [100 mM KCl, 1.8 mM $CaCl_2$, 1 mM $MgCl_2$, and 5 mM Hepes (pH 7.6)]. The oocytes were then washed three times with ND96 solution after labeling and kept on ice until recording. Whole-cell currents were recorded in ND96 solution using similar instruments as the TEVC setup. The fluorescence emission was simultaneously collected by a PIN040-A photodiode (OSI Optoelectronics, Hawthorne, CA) using an Olympus IX51 inverted microscope connected to a patch-clamp head unit/amplifier in voltage clamp mode (Axopatch-1C, Axon Instruments). A PhlatLight LED (Luminus Devices) was used as the light source. The amplified signals were low-pass–filtered at 200 Hz and sampled at 1 kHz using Patchmaster (HEKA, Holliston, MA). All recordings were performed at room temperature (20° to 23°C). C28 (alizarin blue black bg, MP Biomedicals, OH) and RTG (Toronto Research Chemicals) were stored as 100 mM stocks in dimethyl sulfoxide and diluted in bath solutions to working concentrations each experimental day. All other chemicals were obtained from Sigma-Aldrich (St. Louis, MO).

Electrophysiology data analysis

Electrophysiology data were analyzed with MATLAB (MathWorks, MA) and Prism (GraphPad, CA) software. Steady-state current amplitudes at the end of the +40-mV test pulse were used to compare the current amplitudes between wild-type and mutant channels. The *G-V* relationship (with and without drug application) was calculated by measuring the instantaneous tail currents following test pulses to various voltages and normalizing to the maximum tail current in control bath solution for each oocyte. The *G-V* relation was then fitted with a single Boltzmann equation in the form of $G = G_{max}/(1 + \exp(-(V - V_{1/2})/k))$, where G_{max} is the maximum conductance and is set equal to 1 in control condition, V is the test pulse voltage, $V_{1/2}$ is the voltage where channels are at half-maximal activation, and k is the slope factor reflecting the steepness of the curve. $k = RT/zF$, where R is the universal gas constant, T is the absolute temperature, z is the equivalent valence, and F is the Faraday constant. The change in G_{max} after drug application was calculated as $(G_{max,drug} - G_{max,ctrl})/G_{max,ctrl}$, where $G_{max,ctrl} = 1$. To correct for photobleaching, fluorescence signals were first baseline-subtracted by linear fitting and extrapolating the signals at the holding potential preceding each test pulses. The *F-V* relationship was derived after baseline subtraction by obtaining the relative fluorescence change ($\Delta F/F$) at the end of the test pulses to various voltages and normalizing to the maximum fluorescence change. The *F-V* relation was then fitted with a single-component Boltzmann equation (the same as *G-V*) or a two-component Boltzmann equation in the form of $F/F_{max} = A_1/(1 + \exp(-(V - V_{1/2,1})/k_1)) + A_2/(1 + \exp(-(V - V_{1/2,2})/k_2))$, where $A_1 + A_2 = 1$. The fluorescence deactivation time course was fitted with a single-exponential decay function to extract the time constant. Experiments were conducted on at least two separate batches of oocytes to confirm reproducibility. Statistical significance was determined by Student's t test for pairwise comparisons and by one-way analysis of variance (ANOVA) followed by Tukey's post hoc test for multiple comparisons. All average data are presented as mean ± SEM.

Western blot

Membrane and cytoplasmic proteins of oocytes were extracted using the Mem-PER Plus Membrane Protein Extraction Kit (Thermo Fisher Scientific). Equal amounts of protein samples were prepared by adding 2× Laemmli sample buffer (Bio-Rad) and loaded on SDS–polyacrylamide gel electrophoresis gels. After gel electrophoresis, membrane and cytoplasmic proteins were probed by Western blot following standard protocols. KCNQ2 and KCNQ3 proteins were detected with primary antibodies rabbit anti-KCNQ2 (1:1000 dilution; Abcam, ab22897) and rabbit anti-KCNQ3 (1:1000 dilution; Abcam, ab66640), respectively, followed by goat anti-rabbit secondary antibody (1:5000 dilution; Invitrogen, A16110), and visualized using enhanced chemiluminescence (ECL Western Blotting reagent, Thermo Fisher Scientific) and CL-XPosure Film (Thermo Fisher Scientific). β-Actin antibody (1:1000 dilution; Abcam, ab8227) was used to probe for control proteins.

SUPPLEMENTARY MATERIALS

Supplementary material for this article is available at https://science.org/doi/10.1126/sciadv.abo3625

View/request a protocol for this paper from *Bio-protocol*.

REFERENCES AND NOTES

1. M. C. Sanguinetti, M. E. Curran, A. Zou, J. Shen, P. S. Spector, D. L. Atkinson, M. T. Keating, Coassembly of K_VLQT1 and minK (IsK) proteins to form cardiac I_{KS} potassium channel. *Nature* **384**, 80–83 (1996).
2. J. Barhanin, F. Lesage, E. Guillemare, M. Fink, M. Lazdunski, G. Romey, K(V)LQT1 and IsK (minK) proteins associate to form the I(Ks) cardiac potassium current. *Nature* **384**, 78–80 (1996).
3. B. C. Schroeder, S. Waldegger, S. Fehr, M. Bleich, R. Warth, R. Greger, T. J. Jentsch, A constitutively open potassium channel formed by KCNQ1 and KCNE3. *Nature* **403**, 196–199 (2000).
4. H. S. Wang, Z. Pan, W. Shi, B. S. Brown, R. S. Wymore, I. S. Cohen, J. E. Dixon, D. McKinnon, KCNQ2 and KCNQ3 potassium channel subunits: Molecular correlates of the M-channel. *Science* **282**, 1890–1893 (1998).
5. C. Kubisch, B. C. Schroeder, T. Friedrich, B. Lutjohann, A. El-Amraoui, S. Marlin, C. Petit, T. J. Jentsch, KCNQ4, a novel potassium channel expressed in sensory outer hair cells, is mutated in dominant deafness. *Cell* **96**, 437–446 (1999).
6. B. C. Schroeder, M. Hechenberger, F. Weinreich, C. Kubisch, T. J. Jentsch, KCNQ5, a novel potassium channel broadly expressed in brain, mediates M-type currents. *J. Biol. Chem.* **275**, 24089–24095 (2000).
7. J. Sun, R. MacKinnon, Cryo-EM structure of a KCNQ1/CaM complex reveals insights into congenital long QT syndrome. *Cell* **169**, 1042–1050.e9 (2017).
8. J. Sun, R. MacKinnon, Structural basis of human KCNQ1 modulation and gating. *Cell* **180**, 340–347.e9 (2020).
9. D. Wu, K. Delaloye, M. A. Zaydman, A. Nekouzadeh, Y. Rudy, J. Cui, State-dependent electrostatic interactions of S4 arginines with E1 in S2 during Kv7.1 activation. *J. Gen. Physiol.* **135**, 595–606 (2010).
10. J. D. Osteen, C. Gonzalez, K. J. Sampson, V. Iyer, S. Rebolledo, H. P. Larsson, R. S. Kass, KCNE1 alters the voltage sensor movements necessary to open the KCNQ1 channel gate. *Proc. Natl. Acad. Sci. U.S.A.* **107**, 22710–22715 (2010).

11. R. Barro-Soria, S. Rebolledo, S. I. Liin, M. E. Perez, K. J. Sampson, R. S. Kass, H. P. Larsson, KCNE1 divides the voltage sensor movement in KCNQ1/KCNE1 channels into two steps. *Nat. Commun.* **5**, 3750 (2014).
12. M. A. Zaydman, M. A. Kasimova, K. McFarland, Z. Beller, P. Hou, H. E. Kinser, H. Liang, G. Zhang, J. Shi, M. Tarek, J. Cui, Domain-domain interactions determine the gating, permeation, pharmacology, and subunit modulation of the IKs ion channel. *eLife* **3**, e03606 (2014).
13. J. Cui, Voltage-dependent gating: Novel insights from KCNQ1 channels. *Biophys. J.* **110**, 14–25 (2016).
14. K. C. Taylor, P. W. Kang, P. Hou, N. D. Yang, G. Kuenze, J. A. Smith, J. Shi, H. Huang, K. M. White, D. Peng, A. L. George, J. Meiler, R. L. McFeeters, J. Cui, C. R. Sanders, Structure and physiological function of the human KCNQ1 channel voltage sensor intermediate state. *eLife* **9**, e53901 (2020).
15. P. Hou, P. W. Kang, A. D. Kongmeneck, N. D. Yang, Y. Liu, J. Shi, X. Xu, K. M. White, M. A. Zaydman, M. A. Kasimova, G. Seebohm, L. Zhong, X. Zou, M. Tarek, J. Cui, Two-stage electro-mechanical coupling of a KV channel in voltage-dependent activation. *Nat. Commun.* **11**, 676 (2020).
16. P. Hou, J. Eldstrom, J. Shi, L. Zhong, K. McFarland, Y. Gao, D. Fedida, J. Cui, Inactivation of KCNQ1 potassium channels reveals dynamic coupling between voltage sensing and pore opening. *Nat. Commun.* **8**, 1730 (2017).
17. P. Hou, J. Shi, K. M. White, Y. Gao, J. Cui, ML277 specifically enhances the fully activated open state of KCNQ1 by modulating VSD-pore coupling. *eLife* **8**, e48576 (2019).
18. X. Wu, M. E. Perez, S. Y. Noskov, H. P. Larsson, A general mechanism of KCNE1 modulation of KCNQ1 channels involving non-canonical VSD-PD coupling. *Commun. Biol.* **4**, 887 (2021).
19. Y. Lin, S. Z. Grinter, Z. Lu, X. Xu, H. Z. Wang, H. Liang, P. Hou, J. Gao, C. Clausen, J. Shi, W. Zhao, Z. Ma, Y. Liu, K. M. White, L. Zhao, P. W. Kang, G. Zhang, I. S. Cohen, X. Zou, J. Cui, Modulating the voltage sensor of a cardiac potassium channel shows antiarrhythmic effects. *Proc. Natl. Acad. Sci. U.S.A.* **118**, e2024215118 (2021).
20. J. Kurokawa, L. Chen, R. S. Kass, Requirement of subunit expression for cAMP-mediated regulation of a heart potassium channel. *Proc. Natl. Acad. Sci. U.S.A.* **100**, 2122–2127 (2003).
21. J. Kurokawa, H. K. Motoike, J. Rao, R. S. Kass, Regulatory actions of the A-kinase anchoring protein Yotiao on a heart potassium channel downstream of PKA phosphorylation. *Proc. Natl. Acad. Sci. U.S.A.* **101**, 16374–16378 (2004).
22. S. O. Marx, J. Kurokawa, S. Reiken, H. Motoike, J. D'Armiento, A. R. Marks, R. S. Kass, Requirement of a macromolecular signaling complex for beta adrenergic receptor modulation of the KCNQ1-KCNE1 potassium channel. *Science* **295**, 496–499 (2002).
23. M. A. Zaydman, J. R. Silva, K. Delaloye, Y. Li, H. Liang, H. P. Larsson, J. Shi, J. Cui, Kv7.1 ion channels require a lipid to couple voltage sensing to pore opening. *Proc. Natl. Acad. Sci. U.S.A.* **110**, 13180–13185 (2013).
24. D. A. Brown, P. R. Adams, Muscarinic suppression of a novel voltage-sensitive K+ current in a vertebrate neurone. *Nature* **283**, 673–676 (1980).
25. D. A. Brown, G. M. Passmore, Neural KCNQ (Kv7) channels. *Br. J. Pharmacol.* **156**, 1185–1195 (2009).
26. P. Delmas, D. A. Brown, Pathways modulating neural KCNQ/M (Kv7) potassium channels. *Nat. Rev. Neurosci.* **6**, 850–862 (2005).
27. T. J. Jentsch, Neuronal KCNQ potassium channels: Physislogy and role in disease. *Nat. Rev. Neurosci.* **1**, 21–30 (2000).
28. C. Biervert, B. C. Schroeder, C. Kubisch, S. F. Berkovic, P. Propping, T. J. Jentsch, O. K. Steinlein, A potassium channel mutation in neonatal human epilepsy. *Science* **279**, 403–406 (1998).
29. C. Charlier, N. A. Singh, S. G. Ryan, T. B. Lewis, B. E. Reus, R. J. Leach, M. Leppert, A pore mutation in a novel KQT-like potassium channel gene in an idiopathic epilepsy family. *Nat. Genet.* **18**, 53–55 (1998).
30. N. A. Singh, C. Charlier, D. Stauffer, B. R. DuPont, R. J. Leach, R. Melis, G. M. Ronen, I. Bjerre, T. Quattlebaum, J. V. Murphy, M. L. McHarg, D. Gagnon, T. O. Rosales, A. Peiffer, V. E. Anderson, M. Leppert, A novel potassium channel gene, KCNQ2, is mutated in an inherited epilepsy of newborns. *Nat. Genet.* **18**, 25–29 (1998).
31. N. A. Singh, P. Westenskow, C. Charlier, C. Pappas, J. Leslie, J. Dillon, V. E. Anderson, M. C. Sanguinetti, M. F. Leppert, B. P. Consortium, KCNQ2 and KCNQ3 potassium channel genes in benign familial neonatal convulsions: expansion of the functional and mutation spectrum. *Brain* **126**, 2726–2737 (2003).
32. S. Weckhuysen, S. Mandelstam, A. Suls, D. Audenaert, T. Deconinck, L. R. Claes, L. Deprez, K. Smets, D. Hristova, I. Yordanova, A. Jordanova, B. Ceulemans, A. Jansen, D. Hasaerts, F. Roelens, L. Lagae, S. Yendle, T. Stanley, S. E. Heron, J. C. Mulley, S. F. Berkovic, I. E. Scheffer, P. de Jonghe, KCNQ2 encephalopathy: Emerging phenotype of a neonatal epileptic encephalopathy. *Ann. Neurol.* **71**, 15–25 (2012).
33. M. Kato, T. Yamagata, M. Kubota, H. Arai, S. Yamashita, T. Nakagawa, T. Fujii, K. Sugai, K. Imai, T. Uster, D. Chitayat, S. Weiss, H. Kashii, R. Kusano, A. Matsumoto, K. Nakamura, Y. Oyazato, M. Maeno, K. Nishiyama, H. Kodera, M. Nakashima, Y. Tsurusaki, N. Miyake, K. Saito, K. Hayasaka, N. Matsumoto, H. Saitsu, Clinical spectrum of early onset epileptic encephalopathies caused by KCNQ2 mutation. *Epilepsia* **54**, 1282–1287 (2013).
34. G. Orhan, M. Bock, D. Schepers, E. I. Ilina, S. N. Reichel, H. Loffler, N. Jezutkovic, S. Weckhuysen, S. Mandelstam, A. Suls, T. Danker, E. Guenther, I. E. Scheffer, P. De Jonghe, H. Lerche, S. Maljevic, Dominant-negative effects of KCNQ2 mutations are associated with epileptic encephalopathy. *Ann. Neurol.* **75**, 382–394 (2014).
35. V. Barrese, J. B. Stott, I. A. Greenwood, KCNQ-encoded potassium channels as therapeutic targets. *Annu. Rev. Pharmacol. Toxicol.* **58**, 625–648 (2018).
36. F. Miceli, M. V. Soldovieri, P. Ambrosino, L. Manocchio, I. Mosca, M. Taglialatela, Pharmacological targeting of neuronal Kv7.2/3 channels: A focus on chemotypes and receptor sites. *Curr. Med. Chem.* **25**, 2637–2660 (2018).
37. X. Li, Q. Zhang, P. Guo, J. Fu, L. Mei, D. Lv, J. Wang, D. Lai, S. Ye, H. Yang, J. Guo, Molecular basis for ligand activation of the human KCNQ2 channel. *Cell Res.* **31**, 52–61 (2021).
38. A. W. Wang, R. Yang, H. T. Kurata, Sequence determinants of subtype-specific actions of KCNQ channel openers. *J. Physiol.* **595**, 663–676 (2017).
39. T. Li, K. Wu, Z. Yue, Y. Wang, F. Zhang, H. Shen, Structural basis for the modulation of human KCNQ4 by small-molecule drugs. *Mol. Cell.* **81**, 25–37.e4 (2021).
40. R. Y. Kim, M. C. Yau, J. D. Galpin, G. Seebohm, C. A. Ahern, S. A. Pless, H. T. Kurata, Atomic basis for therapeutic activation of neuronal potassium channels. *Nat. Commun.* **6**, 8116 (2015).
41. Y. Zheng, H. Liu, Y. Chen, S. Dong, F. Wang, S. Wang, G. L. Li, Y. Shu, F. Xu, Structural insights into the lipid and ligand regulation of a human neuronal KCNQ channel. *Neuron* **110**, 237–247.e4 (2021).
42. F. Elinder, S. I. Liin, Actions and mechanisms of polyunsaturated fatty acids on voltage-gated ion channels. *Front. Physiol.* **8**, 43 (2017).
43. J. E. Larsson, U. Karlsson, X. Wu, S. I. Liin, Combining endocannabinoids with retigabine for enhanced M-channel effect and improved K_V7 subtype selectivity. *J. Gen. Physiol.* **152**, 202012576 (2020).
44. C. E. Stafstrom, S. Grippon, P. Kirkpatrick, Ezogabine (retigabine). *Nat. Rev. Drug Discov.* **10**, 729–730 (2011).
45. R. Y. Kim, S. A. Pless, H. T. Kurata, PIP2 mediates functional coupling and pharmacology of neuronal KCNQ channels. *Proc. Natl. Acad. Sci. U.S.A.* **114**, E9702–E9711 (2017).
46. A. Etxeberria, I. Santana-Castro, M. P. Regalado, P. Aivar, A. Villarroel, Three mechanisms underlie KCNQ2/3 heteromeric potassium M-channel potentiation. *J. Neurosci.* **24**, 9146–9152 (2004).
47. R. Barro-Soria, Epilepsy-associated mutations in the voltage sensor of KCNQ3 affect voltage dependence of channel opening. *J. Gen. Physiol.* **151**, 247–257 (2019).
48. M. A. Edmond, A. Hinojo-Perez, X. Wu, M. E. Perez Rodriguez, R. Barro-Soria, Distinctive mechanisms of epilepsy-causing mutants discovered by measuring S4 movement in KCNQ2 channels. *eLife* **11**, e77030 (2022).
49. D. Wu, H. Pan, K. Delaloye, J. Cui, KCNE1 remodels the voltage sensor of Kv7.1 to modulate channel function. *Biophys. J.* **99**, 3599–3608 (2010).
50. M. V. Soldovieri, P. Ambrosino, I. Mosca, F. Miceli, C. Franco, L. M. T. Canzoniero, B. Kline-Fath, E. C. Cooper, C. Venkatesan, M. Taglialatela, Epileptic encephalopathy in a patient with a novel variant in the Kv7.2 S2 transmembrane segment: Clinical, genetic, and functional features. *Int. J. Mol. Sci.* **20**, 3382 (2019).
51. M. Pusch, L. Bertorello, F. Conti, Gating and flickery block differentially affected by rubidium in homomeric KCNQ1 and heteromeric KCNQ1/KCNE1 potassium channels. *Biophys. J.* **78**, 211–226 (2000).
52. S. Srivastava, J. S. Cohen, H. Vernon, K. Baranano, R. McClellan, L. Jamal, S. Naidu, A. Fatemi, Clinical whole exome sequencing in child neurology practice. *Ann. Neurol.* **76**, 473–483 (2014).
53. M. Milh, N. Boutry-Kryza, J. Sutera-Sardo, C. Mignot, S. Auvin, C. Lacoste, N. Villeneuve, A. Roubertie, B. Heron, M. Carneiro, A. Kaminska, C. Altuzarra, G. Blanchard, D. Ville, M. A. Barthez, D. Heron, D. Gras, A. Afenjar, N. Dorison, D. Doummar, T. B. de Villemeur, I. An, A. Jacquette, P. Charles, J. Perrier, B. Isidor, L. Vercueil, B. Chabrol, C. Badens, G. Lesca, L. Villard, Similar early characteristics but variable neurological outcome of patients with a de novo mutation of KCNQ2. *Orphanet J. Rare Dis.* **8**, 80 (2013).
54. M. Milh, C. Lacoste, P. Cacciagli, A. Abidi, J. Sutera-Sardo, I. Tzelepis, E. Colin, C. Badens, A. Afenjar, A. D. Coeslier, T. Dailland, G. Lesca, N. Philip, L. Villard, Variable clinical expression in patients with mosaicism for KCNQ2 mutations. *Am. J. Med. Genet. A* **167A**, 2314–2318 (2015).
55. J. D. Symonds, S. M. Zuberi, K. Stewart, A. McLellan, M. O'Regan, S. MacLeod, A. Jollands, S. Joss, M. Kirkpatrick, A. Brunklaus, D. T. Pilz, J. Shetty, L. Dorris, I. Abu-Arafeh, J. Andrew, P. Brink, M. Callaghan, J. Cruden, L. A. Diver, C. Findlay, S. Gardiner, R. Grattan, B. Lang, J. MacDonnell, J. McKnight, C. A. Morrison, L. Nairn, M. M. Slean, E. Stephen, A. Webb, A. Vincent, M. Wilson, Incidence and phenotypes of childhood-onset genetic epilepsies: A prospective population-based national cohort. *Brain* **142**, 2303–2318 (2019).
56. M. J. Main, J. E. Cryan, J. R. Dupere, B. Cox, J. J. Clare, S. A. Burbidge, Modulation of KCNQ2/3 potassium channels by the novel anticonvulsant retigabine. *Mol. Pharmacol.* **58**, 253–262 (2000).
57. A. D. Wickenden, W. Yu, A. Zou, T. Jegla, P. K. Wagoner, Retigabine, a novel anti-convulsant, enhances activation of KCNQ2/Q3 potassium channels. *Mol. Pharmacol.* **58**, 591–600 (2000).

58. A. Schenzer, T. Friedrich, M. Pusch, P. Saftig, T. J. Jentsch, J. Grotzinger, M. Schwake, Molecular determinants of KCNQ (Kv7) K+ channel sensitivity to the anticonvulsant retigabine. *J. Neurosci.* **25**, 5051–5060 (2005).
59. T. V. Wuttke, G. Seebohm, S. Bail, S. Maljevic, H. Lerche, The new anticonvulsant retigabine favors voltage-dependent opening of the Kv7.2 (KCNQ2) channel by binding to its activation gate. *Mol. Pharmacol.* **67**, 1009–1017 (2005).
60. W. Lange, J. Geissendorfer, A. Schenzer, J. Grotzinger, G. Seebohm, T. Friedrich, M. Schwake, Refinement of the binding site and mode of action of the anticonvulsant Retigabine on KCNQ K+ channels. *Mol. Pharmacol.* **75**, 272–280 (2009).
61. Y. Liu, X. Xu, J. Gao, M. M. Naffaa, H. Liang, J. Shi, H. Z. Wang, N. D. Yang, P. Hou, W. Zhao, K. M. White, W. Kong, A. Dou, A. Cui, G. Zhang, I. S. Cohen, X. Zou, J. Cui, A PIP2 substitute mediates voltage sensor-pore coupling in KCNQ activation. *Commun. Biol.* **3**, 385 (2020).
62. H. Zhang, L. C. Craciun, T. Mirshahi, T. Rohacs, C. M. Lopes, T. Jin, D. E. Logothetis, PIP(2) activates KCNQ channels, and its hydrolysis underlies receptor-mediated inhibition of M currents. *Neuron* **37**, 963–975 (2003).
63. Y. Haitin, B. Attali, The C-terminus of Kv7 channels: A multifunctional module. *J. Physiol.* **586**, 1803–1810 (2008).
64. P. W. Kang, A. M. Westerlund, J. Shi, K. M. White, A. K. Dou, A. H. Cui, J. R. Silva, L. Delemotte, J. Cui, Calmodulin acts as a state-dependent switch to control a cardiac potassium channel opening. *Sci. Adv.* **6**, eabd6798 (2020).
65. L. Shamgar, L. Ma, N. Schmitt, Y. Haitin, A. Peretz, R. Wiener, J. Hirsch, O. Pongs, B. Attali, Calmodulin is essential for cardiac IKS channel gating and assembly: Impaired function in long-QT mutations. *Circ. Res.* **98**, 1055–1063 (2006).
66. F. Bezanilla, E. Perozo, E. Stefani, Gating of Shaker K+ channels: II. The components of gating currents and a model of channel activation. *Biophys. J.* **66**, 1011–1021 (1994).
67. W. N. Zagotta, T. Hoshi, R. W. Aldrich, Shaker potassium channel gating. III: Evaluation of kinetic models for activation. *J. Gen. Physiol.* **103**, 321–362 (1994).
68. J. L. Ledwell, R. W. Aldrich, Mutations in the S4 region isolate the final voltage-dependent cooperative step in potassium channel activation. *J. Gen. Physiol.* **113**, 389–414 (1999).
69. J. J. Lacroix, H. C. Hyde, F. V. Campos, F. Bezanilla, Moving gating charges through the gating pore in a Kv channel voltage sensor. *Proc. Natl. Acad. Sci. U.S.A.* **111**, E1950–E1959 (2014).
70. J. J. Lacroix, S. A. Pless, L. Maragliano, F. V. Campos, J. D. Galpin, C. A. Ahern, B. Roux, F. Bezanilla, Intermediate state trapping of a voltage sensor. *J. Gen. Physiol.* **140**, 635–652 (2012).
71. J. J. Lacroix, F. Bezanilla, Control of a final gating charge transition by a hydrophobic residue in the S2 segment of a K+ channel voltage sensor. *Proc. Natl. Acad. Sci. U.S.A.* **108**, 6444–6449 (2011).
72. M. V. Soldovieri, P. Ambrosino, I. Mosca, M. De Maria, E. Moretto, F. Miceli, A. Alaimo, N. Iraci, L. Manocchio, A. Medoro, M. Passafaro, M. Taglialatela, Early-onset epileptic encephalopathy caused by a reduced sensitivity of Kv7.2 potassium channels to phosphatidylinositol 4,5-bisphosphate. *Sci. Rep.* **6**, 38167 (2016).
73. P. Zhou, H. Yu, M. Gu, F. J. Nan, Z. Gao, M. Li, Phosphatidylinositol 4,5-bisphosphate alters pharmacological selectivity for epilepsy-causing KCNQ potassium channels. *Proc. Natl. Acad. Sci. U.S.A.* **110**, 8726–8731 (2013).
74. D. L. Prole, N. V. Marrion, Ionic permeation and conduction properties of neuronal KCNQ2/KCNQ3 potassium channels. *Biophys. J.* **86**, 1454–1469 (2004).
75. J. J. Millichap, K. L. Park, T. Tsuchida, B. Ben-Zeev, L. Carmant, R. Flamini, N. Joshi, P. M. Levisohn, E. Marsh, S. Nangia, V. Narayanan, X. R. Ortiz-Gonzalez, M. C. Patterson, P. L. Pearl, B. Porter, K. Ramsey, E. L. McGinnis, M. Taglialatela, M. Tracy, B. Tran, C. Venkatesan, S. Weckhuysen, E. C. Cooper, KCNQ2 encephalopathy: Features, mutational hot spots, and ezogabine treatment of 11 patients. *Neurol. Genet.* **2**, e96 (2016).
76. C. Gomis-Perez, J. Urrutia, A. Marce-Grau, C. Malo, E. Lopez-Laso, A. Felipe-Rucian, M. Raspall-Chaure, A. Macaya, A. Villarroel, Homomeric Kv7.2 current suppression is a common feature in KCNQ2 epileptic encephalopathy. *Epilepsia* **60**, 139–148 (2019).

Acknowledgments

Funding: This work was supported by NIH grants R01 HL126774 (to J.C.), R01 GM104991 (to J.M.N.), and R01 HL142520 (to J.M.N.); U.S.-Israel Binational Science Foundation research grant 2019159 (to J.C.); Canadian Institutes of Health Research operating grant (to H.T.K., MOP 142482); Mitacs Acceleration Fellowship (to R.K., IT 16776); and The McDonnell Center for Cellular and Molecular Neurobiology Post-Doctoral Fellowship (to L.Z.). **Author contributions:** Conceptualization: N.-D.Y., H.T.K., and J.C. Methodology: N.-D.Y., R.K., L.Z., J.L., H.T.K., and J.C. Investigation: N.-D.Y., R.K., L.Z., J.L., P.W.K., A.K.D., K.M.W., J.S., H.T.K., and J.C. Visualization: N.-D.Y., R.K., L.Z., P.W.K., H.T.K., and J.C. Supervision: H.T.K. and J.C. Writing—original draft: N.-D.Y., H.T.K., and J.C. Writing—review and editing: N.-D.Y., R.K., P.W.K., J.M.N., H.T.K., and J.C. **Competing interests:** J.S. and J.C. are cofounders of a startup company VivoCor LLC, which is targeting I_{Ks} for the treatment of cardiac arrhythmia. The other authors declare that they have no competing interests. **Data and materials availability:** All data needed to evaluate the conclusions in the paper are present in the paper and/or the Supplementary Materials.

Submitted 29 January 2022
Accepted 7 June 2022
Published 20 July 2022
10.1126/sciadv.abo3625